



RESEARCH ARTICLE

Astrocytes in stress accumulate lipid droplets

Tina Smolič¹ | Petra Tavčar¹ | Anemari Horvat^{1,2} | Urška Černe¹ |
 Ana Halužan Vasle¹ | Larisa Tratnjek³ | Mateja Erdani Kreft³ | Nicole Scholz⁴ |
 Maja Matis^{5,6} | Toni Petan⁷ | Robert Zorec^{1,2}  | Nina Vardjan^{1,2} 

¹Laboratory of Neuroendocrinology-Molecular Cell Physiology, Faculty of Medicine, Institute of Pathophysiology, University of Ljubljana, Ljubljana, Slovenia

²Laboratory of Cell Engineering, Celica Biomedical, Ljubljana, Slovenia

³Faculty of Medicine, Institute of Cell Biology, University of Ljubljana, Ljubljana, Slovenia

⁴Division of General Biochemistry, Medical Faculty, Rudolf Schönheimer Institute of Biochemistry, Leipzig University, Leipzig, Germany

⁵Medical Faculty, Institute of Cell Biology, University of Münster, Münster, Germany

⁶Cells in Motion Interfaculty Centre, University of Münster, Münster, Germany

⁷Department of Molecular and Biomedical Sciences, Jožef Stefan Institute, Ljubljana, Slovenia

Correspondence

Nina Vardjan, Laboratory of Neuroendocrinology-Molecular Cell Physiology, Institute of Pathophysiology, Faculty of Medicine, University of Ljubljana, 1000 Ljubljana, Slovenia.
 Email: nina.vardjan@mf.uni-lj.si

Funding information

European Cooperation in Science and Technology (COST) Action, Grant/Award Numbers: CM1207, CA18133, CA19105; German Research Foundation, Grant/Award Numbers: EXC-1003, FOR 2149/P01 (SCHO 1791/1-2), CRC 1423, project number 421152132, subproject B06; Slovenian Research Agency, Grant/Award Numbers: P1-0207, J7-1818, P3-0310, J3-2523, BI-DE/18-19-015, J3-9266, J7-2594

Abstract

When the brain is in a pathological state, the content of lipid droplets (LDs), the lipid storage organelles, is increased, particularly in glial cells, but rarely in neurons. The biology and mechanisms leading to LD accumulation in astrocytes, glial cells with key homeostatic functions, are poorly understood. We imaged fluorescently labeled LDs by microscopy in isolated and brain tissue rat astrocytes and in glia-like cells in *Drosophila* brain to determine the (sub)cellular localization, mobility, and content of LDs under various stress conditions characteristic for brain pathologies. LDs exhibited confined mobility proximal to mitochondria and endoplasmic reticulum that was attenuated by metabolic stress and by increased intracellular Ca²⁺, likely to enhance the LD-organelle interaction imaged by electron microscopy. When de novo biogenesis of LDs was attenuated by inhibition of DGAT1 and DGAT2 enzymes, the astrocyte cell number was reduced by ~40%, suggesting that in astrocytes LD turnover is important for cell survival and/or proliferative cycle. Exposure to noradrenaline, a brain stress response system neuromodulator, and metabolic and hypoxic stress strongly facilitated LD accumulation in astrocytes. The observed response of stressed astrocytes may be viewed as a support for energy provision, but also to be neuroprotective against the stress-induced lipotoxicity.

Abbreviations: ADFP, adipose differentiation-related protein; ALS, amyotrophic lateral sclerosis; ANLS, astrocyte-neuron lactate shuttle; ANP, atrial natriuretic peptide; AR, adrenergic receptor; Atip, atipamezole; ATP, adenosine triphosphate; BSA, bovine serum albumin; cAMP, cyclic adenosine monophosphate; CNS, central nervous system; CREB, cyclic AMP-response element-binding protein; DAPI, 4,6-diamidino-2-phenylindole; Dex, dexmedetomidine; DGAT, diacylglycerol acyltransferase; ECS, extracellular solution; ER, endoplasmic reticulum; FFA, free fatty acid; FWHM, full width at half maximum; GFAP, glial fibrillary acidic protein; GFP, green fluorescent protein; Iso, isoprenaline; LAMP1, lysosomal-associated membrane protein 1; LC3, microtubule-associated protein 1 light chain 3; LD, lipid droplet; MD, maximal displacement; Mi, mitochondrion; NA, noradrenaline; OA, oleic acid; PE, phenylephrine; Prop, propranolol; rER, rough endoplasmic reticulum; ROS, reactive oxygen species; RT, room temperature; SIM, structured illumination microscopy; SSLVs, small synaptic-like vesicles; TAG, triacylglycerol; TEM, transmission electron microscopy; Tera, terazosin; TL, track length; vGLUT1, vesicular glutamate transporter 1.

This is an open access article under the terms of the Creative Commons Attribution-NonCommercial-NoDerivs License, which permits use and distribution in any medium, provided the original work is properly cited, the use is non-commercial and no modifications or adaptations are made.

© 2021 The Authors. *Glia* published by Wiley Periodicals LLC.

KEYWORDS

adrenergic receptors, astrocytes, lipid droplets, metabolic/hypoxic stress, noradrenaline

1 | INTRODUCTION

Astrocytes, an abundant subtype of neuroglia, constitute a morphologically and physiologically heterogeneous cell population involved in a variety of homeostatic functions in the central nervous system (CNS; Verkhratsky & Nedergaard, 2018). This includes regulation of the energy metabolism in the CNS, where astrocytes and neurons may operate as a tightly coupled metabolic unit (Dienel, 2019b; Magistretti & Allaman, 2018). Although lipids represent the most important structural component of the CNS membranes, accounting for approximately half of the brain tissue dry weight (Barber & Raben, 2019; Tracey, Steyn, Wolvetang, & Ngo, 2018), studies in the past decades have mainly focused on the glucose energy metabolism in the CNS (Bélanger, Allaman, & Magistretti, 2011; Dienel, 2012, 2019a, 2019b; Falkowska et al., 2015; Magistretti & Allaman, 2018). Therefore, the knowledge of how lipids contribute to the CNS energy metabolism remains largely unknown.

Astrocyte processes surround blood capillaries and neuronal synapses (Tsacopoulos & Magistretti, 1996). Thus, they are ideally positioned to transport nutrients, such as glucose, free fatty acids (FFAs), and ketone bodies, from the systemic circulation to neurons and to store blood-derived glucose in the form of glycogen (Brown & Ransom, 2007). Under stimulation (e.g., glutamatergic or noradrenergic stimulation during times of stress), when the metabolic demands of neural cells are increased, despite normal oxygen levels, astrocytes metabolize glycogen to glucose and further into lactate in the process of aerobic glycolysis (Bélanger et al., 2011; Dienel & Cruz, 2016; Pellerin & Magistretti, 1994). Lactate is considered to be used by astrocytes as a fuel to spare glucose for neurons (DiNuzzo, Mangia, Maraviglia, & Giove, 2010; Dinuzzo, Mangia, Maraviglia, & Giove, 2012) or it is released from astrocytes. When released, lactate may exit CNS and enter the systemic circulation (Dienel, 2012), it may enter neurons, where it is oxidized (i.e., the astrocyte-neuron lactate shuttle [ANLS] hypothesis; Bélanger et al., 2011), or it may act as a signaling molecule by binding to lactate receptors (Barros & Deitmer, 2010; de Castro Abrantes et al., 2019; Mosienko, Teschemacher, & Kasparov, 2015; Tang et al., 2014; Vardjan et al., 2018).

Recent studies (Ioannou et al., 2019; L. Liu, MacKenzie, Putluri, Maletić-Savatić, & Bellen, 2017) suggest glial-neuronal coupling of glucose and lipid metabolism during increased neural cell activity. Studies utilizing an in vitro astrocyte-neuron co-culture system derived from *Drosophila* tissue has linked glial lactate transport to neurons via ANLS to increased FFA production in neurons (Ioannou et al., 2019; L. Liu et al., 2017). Neurons are vulnerable to reactive oxygen species (ROS) generated during β -oxidation of FFAs (Bruce, Zsombok, & Eckel, 2017), which is why excessive FFAs can be lipotoxic for neurons. To avoid lipotoxicity it is believed that FFAs are transferred from neurons to glial cells, particularly astrocytes, where they are stored in LDs (Ioannou

et al., 2019). LDs are storage organelles composed of a core of neutral lipids containing triacylglycerols (TAGs) and sterol esters surrounded by a phospholipid monolayer and various associated proteins. Their multi-step assembly involves ER-resident proteins, including diacylglycerol acyltransferases (DGAT1 and DGAT2), which catalyze the final step in TAG synthesis (Pol, Gross, & Parton, 2014; Welte, 2009). LD-stored FFAs can then be used by astrocytes for energy production in β -oxidation (Ioannou et al., 2019). It remains to be elucidated whether LDs also supply astrocytes with lipids (FFA and cholesterol) for the synthesis of membranes and/or with lipids that act as signaling molecules (mediators), as suggested in other cell types (Rambold, Cohen, & Lippincott-Schwartz, 2015; Walther & Farese, 2012).

At rest, LDs are observed in the CNS only at low levels (Etschmaier et al., 2011). In contrast, when the CNS is in a pathological state (i.e., cancer, neurodegenerative diseases, and ageing), the content of LDs in the CNS is increased, predominantly in glial cells (astrocytes, microglia) and much less in neurons (Bailey et al., 2015; Kis, Barti, Lippai, & Sass, 2015; L. Liu et al., 2015; Marschallinger et al., 2020). LDs have been shown to accumulate in tumors, such as astrocytomas (Barba, Cabañas, & Arús, 1999; Opstad, Bell, Griffiths, & Howe, 2008; Rémy et al., 1997; Zoula et al., 2003), in the brains of patients with Alzheimer's disease and 3xTg-AD mice (Derk et al., 2018; Gómez-Ramos & Asunción Morán, 2007; Hamilton et al., 2015) as well as in patients with Parkinson's disease, where LDs were proposed to be the sites of α -synuclein aggregation (Cole et al., 2002). Moreover, LDs have been linked to motor neuron diseases, including amyotrophic lateral sclerosis (ALS; Chaves-Filho et al., 2019; Pennetta & Welte, 2018; Velebit et al., 2020), multiple sclerosis (Grajchen, Hendriks, & Bogie, 2018; Kamermans et al., 2019; Ponath et al., 2017), and hereditary spastic paraplegia (Fowler, Garcia-Pardo, Simpson, & O'Sullivan, 2019; Papadopoulos et al., 2015; Renvoisé et al., 2016).

The characteristics of LDs and the mechanisms leading to LD accumulation in astrocytes are unclear. In non-adipose cells, LD accumulation has been associated with various stress stimuli and stress-related lipotoxicity (Henne, Reese, & Goodman, 2018; Petan, Jarc, & Jusovic, 2018). Nutrient deprivation and hypoxia are common stressors in many CNS pathologies and might be a trigger for LD accumulation in glial cells to protect neurons from stress-induced lipotoxicity (Ioannou et al., 2019; L. Liu et al., 2017).

The nature and dynamics of LD biology in astrocytes are poorly understood. It was studied here by using transmission electron microscopy and fluorescence microscopy in combination with Nile Red or BODIPY^{493/503} labeling of LDs, in isolated and brain tissue rat astrocytes and in glia-like cells of *Drosophila* brain. We found that LDs in resting astrocytes are organelles of ~450 nm in diameter localized in the soma and processes in the proximity of mitochondria and endoplasmic reticulum (ER). LDs displayed limited mobility, which was further reduced by stimulation-evoked increase in intracellular Ca²⁺ levels



and metabolic stress. Inhibition of de novo biogenesis of LDs reduced astrocyte cell number, implying that LD turnover in astrocytes is important for cell survival and/or proliferative cycle. The cellular content of LDs increased by >2-fold in astrocytes exposed to metabolic stress (nutrient deprivation, excess of extracellular FFAs and lactate) or hypoxic stress (1% pO₂), indicating LD accumulation. A similar increase in LD accumulation was observed upon chronic exposure of astrocytes to NA, the effects of which were mediated by activation of β- and α₂-adrenergic receptors (ARs). Taken together, our results reveal that NA and metabolic and hypoxic stress, typically present in various CNS pathologies, promote LD accumulation in astrocytes.

2 | MATERIALS AND METHODS

Unless stated otherwise, all chemicals were of the highest purity available and obtained from Sigma-Aldrich (Merck KGaA, Darmstadt, Germany).

All animal procedures were conducted in accordance with the International Guiding Principles for Biomedical Research Involving Animals developed by the Council for International Organizations of Medical Sciences and Animal Protection Act (Official Gazette of the RS, No. 38/13). The experimental protocol was approved by The Administration of the Republic of Slovenia for Food Safety, Veterinary and Plant Protection (Republic of Slovenia, Ministry of Agriculture, Forestry and Food, Dunajska Cesta 22, 1000 Ljubljana), document no. U34401-47/2014/7 and U34401-48/2014/7, signed by Barbara Tomše, DVM.

2.1 | Cell culture

Primary cultures of astrocytes were prepared from the cortex of neonatal Wistar rats (2–3 days old) as described previously (Schwartz & Wilson, 1992). Cultures of isolated astrocytes were maintained in high-glucose Dulbecco's modified Eagle's medium supplemented with 10% fetal bovine serum, 1 mM sodium pyruvate, 2 mM L-glutamine, 5 U/ml penicillin, and 5 μg/ml streptomycin in 5% CO₂/95% air at 37°C. Cells were plated on 22-mm diameter coverslips coated with poly-L-lysine. Experiments were performed after 24 hr, when cells reached 60–70% confluency to avoid confluence-induced LD generation (Quintero, Cabañas, & Arús, 2007).

2.2 | Organotypic brain slice cultures

Organotypic brain slice cultures were prepared from 2- to 4-month-old Wistar rats. The rats were euthanized with 100% CO₂ (Messer Slovenia, Ruše, Slovenia) inhalation for ~5 min. After decapitation, the brain was removed and transferred to an ice-cold dissection medium containing Hanks' balanced salt solution, supplemented with 41.55 mM D-glucose and antibiotic–antimycotic solution (100 U/ml penicillin, 100 μg/ml streptomycin, and 0.25 μg/ml amphotericin B; Gibco, Thermo Fisher Scientific, Waltham, MA, USA). After removing cerebellum and the frontal part of the brain, the brain was glued to the specimen holder of a vibratome (VT1000S; Leica Biosystems,

Wetzlar, Germany) and coronal slices (~200 μm) were cut. The brain slices were placed onto a 0.45-μm pore LCR membrane positioned on the top of the membrane insert with a pore diameter of 0.4 μm (Sarstedt, Nümbrecht, Germany) and cultured in 6-well plates with 1 ml/well of the growth medium containing minimum essential medium (Thermo Fisher Scientific) and Earl's balanced salt solution in a 2:1 ratio, supplemented with 4.2% heat-inactivated horse serum (Thermo Fisher Scientific), 1 mM L-glutamine, 21 mM D-glucose and antibiotic–antimycotic solution (100 U/ml penicillin, 100 μg/ml streptomycin, and 0.25 μg/ml amphotericin B; Gibco, Thermo Fisher Scientific) at 37°C in 5% CO₂/95% air. Brain slices were cultured for up to 5 days, and the medium was changed every 2 days.

2.3 | *Drosophila melanogaster* stocks and crosses

Drosophila melanogaster flies were raised at 25°C on standard cornmeal and molasses medium. The following strains were used in this study: *repo-Gal4* (Xiong, Okano, Patel, Blendy, & Montell, 1994), *UAS-L10a-EGFP* (Huang, Ainsley, Reijmers, & Jackson, 2013), and wild-type (*w¹¹¹⁸*). *repo-Gal4 > UAS-L10a-EGFP* animals were used to outline glial cells in the adult CNS.

2.4 | Experimental solutions

2.4.1 | Cell cultures

Extracellular solution (ECS) for cell cultures contained 10 mM D-glucose, 131.8 mM NaCl, 5 mM KCl, 10 mM HEPES, 1.8 mM CaCl₂, and 2 mM MgCl₂. ECS for cell cultures without glucose contained 135 mM NaCl, 5 mM KCl, 10 mM HEPES, 1.8 mM CaCl₂, and 2 mM MgCl₂.

2.4.2 | Organotypic brain slice cultures

ECS for tissue cultures contained 10 mM D-glucose, 123 mM NaCl, 2.5 mM KCl, 1.3 mM NaH₂PO₄, 26.2 mM NaHCO₃, 1.3 mM MgCl₂, and 2.5 mM CaCl₂. ECS for tissue cultures without glucose contained 128 mM NaCl, 2.5 mM KCl, 1.3 mM NaH₂PO₄, 26.2 mM NaHCO₃, 1.3 mM MgCl₂, and 2.5 mM CaCl₂.

The pH of extracellular solutions was adjusted to 7.2 and the osmolality was ~300 mOsm, measured with a freezing point depression osmometer (Osmomat030; Gonotech, Berlin, Germany).

2.5 | Stress induction via reagents and hypoxia

2.5.1 | Cell cultures and organotypic brain slice cultures

Cell and tissue cultures were exposed to the growth medium (control), ECS with 10 mM glucose or without glucose (starvation), 300 μM

oleic acid (OA; excess of FFA), 20 mM sodium L-lactate (excess of L-lactate), 40 mM D-sorbitol (osmolality test), 100 μ M noradrenaline (α -/ β -AR agonist), 100 μ M isoprenaline (β -AR agonist), 50 nM dexmedetomidine (α_2 -AR agonist), or 100 μ M phenylephrine (α_1 -AR agonist) in growth medium for 24 hr at 37°C. In some experiments, astrocytes were exposed to 100 μ M noradrenaline in growth medium in the presence of AR antagonists, 1 μ M (cell culture), or 10 μ M (tissue slices) propranolol (β -AR antagonist), 10 μ M atipamezole (α_2 -AR antagonist) and 10 μ M terazosin (α_1 -AR antagonist) for 24 hr at 37°C. Before exposure to noradrenaline, cell cultures, and brain slices were pretreated with selective AR antagonists for 30 min and 1 hr, respectively. In experiments with AR agonists and antagonists, all reagents were reapplied after 8–12 hr of a 24-hr incubation.

To induce hypoxia, cell, and tissue cultures were placed in a hypoxic chamber (Billups-Rothenberg, Del Mar, CA), flushed for 4 min with a gas mixture consisting of 1% O₂/5% CO₂/94% N₂ at the beginning and after 2 hr of the experiment and incubated for 24 hr at 37°C in a humidified atmosphere.

To prevent the synthesis of TAGs and LD biogenesis, cultured astrocytes were 24 hr after seeding supplied with fresh growth medium or extracellular solution without glucose with or without the presence of 10 μ M DGAT1 inhibitor T863 and 10 μ M DGAT2 inhibitor PF-06424439 and incubated for 24 hr at 37°C. Cells were counted with a Scepter™ cell counter using a 60 μ m Scepter™ sensor. The results were exported (Scepter™ Software Pro 2.1, Merck Millipore, Darmstadt, Germany) and cells counted based on cell diameters ranging between 8.25 μ m (low marker) and 24.08 μ m (high marker). The obtained values were normalized to the controls (growth medium).

2.5.2 | *Drosophila melanogaster*

After eclosion *repo-Gal4 > UAS-L10a-EGFP* flies were kept on standard medium for 3–5 days. Subsequently, a group of flies was transferred to fresh standard medium for 24 hr (control), while a second group of flies was transferred to vials containing 1% agar and exposed to hypoxic conditions (1% O₂/5% CO₂/94% N₂) for 24 hr using a hypoxic chamber (Billups-Rothenberg; hypoxia + starvation). All experiments were performed at room temperature (RT) in duplicate (two separate vials for each group).

2.6 | Cell and tissue staining

2.6.1 | Cell cultures

Astrocytes growing on coverslips were fixed in 4% formaldehyde (Thermo Fisher Scientific) for 15 min at RT, washed with phosphate-buffered saline (PBS), and treated with 10% goat serum for 1 hr at 37°C. The cells were incubated with primary antibodies overnight at 4°C: rabbit anti-adipose differentiation-related protein (ADFP/perilipin-2; 1:1,000; Abcam Cat# ab108323, RRID:AB_10863476), rabbit anti-D-serine (D-serine; 1:1,000; Gemacbio Cat# APO41, RRID:AB_2314275),

rabbit anti-vesicular glutamate transporter 1 (vGLUT1; 1:1,000; Synaptic Systems Cat# 135303, RRID:AB_887875), rabbit anti-atrial natriuretic peptide (ANP; 1:3,000; Abcam Cat# ab14348, RRID:AB_301128), rabbit anti-lysosomal-associated membrane protein 1 (LAMP1; 1:100; Abcam Cat# ab24170, RRID:AB_775978) and mouse anti-microtubule-associated protein 1 light chain 3 (LC3; 1:100; MBL International Cat# M152-3, RRID:AB_1279144). Excess primary antibody was washed off, and the cells were stained with secondary anti-mouse or anti-rabbit antibodies conjugated to Alexa Fluor⁴⁸⁸ (1:500; Thermo Fisher Scientific) for 45 min at 37°C. Afterward, the cells were stained with 100 nM Nile Red (Invitrogen, Molecular Probes, Thermo Fisher Scientific, Eugene, OR), a fluorescent marker for neutral lipids (labels LDs), for 5 min at RT and then mounted onto glass slides using SlowFade Gold antifade agent (Invitrogen, Molecular Probes, Thermo Fisher Scientific). To label the ER, cells were transfected with green fluorescent protein-tagged ER protein Sec61 β (GFP-Sec61 β ; Addgene plasmid #15108; deposited by T. Rapoport) using FuGene 6 transfection reagent according to the manufacturer's instructions (Promega, Madison, WI, USA). Acidic compartments and mitochondria were stained in living astrocytes with fluorescent dyes, LysoTracker Green DND-26 (400 nM; Invitrogen, Molecular Probes, Thermo Fisher Scientific) and MitoTracker Green FM or MitoTracker Red CMXRos (50 nM; Invitrogen, Molecular Probes, Thermo Fisher Scientific), respectively, and then with Nile Red (50 nM) or BODIPY^{493/503} (1 μ g/ml; BODIPY 493/503, Invitrogen, Molecular Probes, Thermo Fisher Scientific), fluorescent markers for neutral lipids (label LDs), according to the manufacturer's instructions.

2.6.2 | Organotypic brain slice cultures

Tissue cultures were fixed in 4% formaldehyde (Thermo Fisher Scientific) for 4 hr at RT, washed with PBS, and incubated in 20% bovine serum albumin (BSA)/0.5% Triton-X-100 overnight at 4°C. After blocking and permeabilization, slices were incubated with primary anti-mouse glial fibrillary acidic protein antibodies (GFAP; 1:100; Sigma-Aldrich Cat# G3893, RRID:AB_477010) in 2% BSA/0.25% Triton-X-100 for 24 hr at 4°C. After washing to remove excess primary antibodies, the slices were stained with secondary anti-mouse antibodies conjugated to Alexa Fluor⁵⁴⁶ (1:600; Thermo Fisher Scientific) for 2 hr at RT. Excess antibodies were washed off and the slices were stained with BODIPY^{493/503} (5 μ g/ml) for 20 min at RT and 4,6-diamidino-2-phenylindole (30 μ M; DAPI; Invitrogen, Molecular Probes) for 5 min at RT. The slices were then mounted onto glass slides using Vectashield fluorescent mounting medium (Vector Laboratories, Burlingame, CA, USA).

2.6.3 | *Drosophila* brains

Brains of 3–5 days old male flies were analyzed. Brains were dissected in ice-cold PBS and collected in 24-well plate inserts containing ice-cold PBS. Fixation was done with 4% formaldehyde and 0.5% Triton X-100 in PBS for 45 min at RT. Brains were then rinsed twice and



washed 3 × 15 min in PBS while shaking gently before being treated with 1 µg/ml Nile Red in PBS (hypoxia and starvation assay) or simultaneously with 1 µg/ml BODIPY^{493/503} in PBS (colocalization assessment) for 30 min at RT. Brains were rinsed once with PBS and immediately mounted onto glass slides using Vectashield mounting medium with DAPI (Vector Laboratories, Inc., Burlingame, CA, USA). Nile Red and BODIPY^{493/503} colocalization analysis was done on 5-day-old wild-type male flies.

2.7 | Confocal microscopy

Cultured cells and brain tissue slices were imaged with a fluorescence confocal microscope LSM 780 (Zeiss, Jena, Germany) using a plan apochromatic oil-immersion objective 40×/numerical aperture 1.3 or 63×/numerical aperture 1.4 (Zeiss). Confocal images were obtained with a 488 nm argon laser (BODIPY^{493/503}), 561 nm diode-pumped solid-state laser (Alexa Fluor⁵⁴⁶, Nile Red), and 405 nm (DAPI) diode laser excitation. The fluorescence emissions were filtered using 500–550 nm, 565–630 nm, and 413–463 nm band-pass filters.

Images of *Drosophila* brains were recorded with an inverted Zeiss LSM800 confocal microscope with a Plan-Apochromat 63×/1.40 Oil DIC M27 objective (Zeiss) using 488 nm and 561 nm diode laser excitation. Emission spectra were acquired sequentially with 410–514 nm (EGFP or BODIPY^{493/503}) and 564–700 nm (Nile Red) bandpass emission filters. For LD analysis, Z-stacks with 10 µm interval and 50 µm pinhole were recorded for each brain hemisphere.

Live-cell imaging was performed on an LSM 510 META laser scanning microscope (Zeiss) equipped with a Plan-Neofluar 63×/1.4 oil DIC immersion objective (Zeiss). Confocal images were obtained with a 488 nm Ar-ion laser (LysoTracker, MitoTracker Green) and a 543 nm He-Ne laser (Nile Red), and the fluorescence emissions were collected using 505–530 nm band-pass and 560 nm long-pass emission filters, respectively.

2.8 | Structured illumination microscopy

In some experiments, BODIPY^{493/503}-labelled LDs were imaged in fixed cells and the distances between BODIPY^{493/503}-labeled LDs and MitoTracker Red CMXRos-labeled mitochondria in living cells were measured as reported (Singh et al., 2014) by super-resolution structured illumination microscopy (SIM; ELYRA PS.1; Zeiss) using an oil-immersion plan apochromatic objective 63×/numerical aperture 1.4 DIC, a 488 nm and 561 nm laser line excitation, an emission band-pass filter 495–575 nm (BODIPY^{493/503}) and 570–650 nm (MitoTracker Red) and an EMCCD camera (Andor iXon 885; Belfast, UK). The thickness of each optical slice of a Z-stack was 500 nm.

2.9 | Transmission electron microscopy

Astrocytes growing on coverslips were fixed with a solution of 2% (w/v) formaldehyde and 2.5% (v/v) glutaraldehyde (Serva, Heidelberg,

Germany) in 0.1 M cacodylate buffer, pH 7.4, at 37°C for 10 min and then incubated on ice for additional 30 min. After fixation, samples were rinsed in 0.1 M sodium cacodylate supplemented with 3 mM CaCl₂ (pH 7.4) on ice (3 times for 3 min). Samples were then post-fixed in 1% osmium tetroxide (Serva), 0.8% potassium ferrocyanide, and 3 mM CaCl₂ in 0.1 M sodium cacodylate (pH 7.4) for 1 hr at RT. After rinsing in ice-cold distilled water (3 times for 3 min), samples were incubated overnight in 2% uranyl acetate at 4°C. Samples were then dehydrated in a graded series of ethanol (30% EtOH 3 min, 50% EtOH 3 min, 70% EtOH 3 min, 90% EtOH 5 min, 100% EtOH 2 × 5 min) and embedded in Epon (Serva). Epon semi-thin sections were stained with 1% toluidine blue and 2% borate in distilled water and examined with a Nikon Eclipse TE microscope. Ultrathin sections were contrasted with uranyl acetate and lead citrate and observed with a transmission electron microscope (Philips CM100, [Philips, Eindhoven, Netherlands]), operation voltage 80 kV, equipped with CCD camera (AMT, Danvers, MA, USA). The thickness of ultra-thin slice was 70 µm.

2.10 | Lipid droplet mobility and analysis

Living cultured astrocytes were stained with 50 nM Nile Red solution for 5 min at RT, washed with ECS, mounted into the recording chamber, and transferred to the confocal microscope (LSM 510) for live imaging. Time-lapse fluorescence images were obtained every 2 s for 1 min (30 frames) before and 3 min (90 frames) after stimulation with 100 µM adenosine triphosphate (ATP). The mobility of LDs was analyzed by ParticleTR software (Celica Biomedical, Ljubljana, Slovenia) in exported TIFF files (Potokar, Kreft, Pangrsic, & Zorec, 2005). Approximately 50 randomly selected LDs were tracked per cell and the track length (TL; the pathway that individual LDs traveled), the maximal displacement (MD; the farthest translocation of the LDs), and the velocity were determined for 60-s epochs. For the analysis of LD mobility, only cells containing LDs were taken into account (35% ± 1% of astrocytes in control conditions contained LDs).

2.11 | Image analysis

2.11.1 | Colocalization studies

The colocalization of green and red fluorescence pixels on each image was determined using custom-made Matlab Software as described (Kreft, Milisav, Potokar, & Zorec, 2004). Briefly, the program counted all red, all green, and all colocalized pixels in the image. The colocalization was calculated as a percentage of colocalized pixels compared with all red pixels. The threshold intensity for the colocalized pixels was 20% (51 AU) of the maximal fluorescence intensity (256 AU). The masks (representing an overlay area of the green and the red fluorescence pixels in an image) were prepared using the LSM 510 META Histo tool by setting the threshold intensity at 20% (51 AU) of the maximal red and green fluorescence signals (256 AU) in the original images.

2.11.2 | LD and mitochondria distance measurement

The distance between LDs and mitochondria was measured as the distance between the peaks of the green (LDs) and the red (mitochondria) fluorescence intensity profiles in a single plane SIM image using Zen software, as described (P. Singh et al., 2014). For analysis, only LDs in focus and in close proximity to the nearest mitochondrion were taken into account.

2.11.3 | Determination of LD area, perimeter, diameter, and number

Cross-sectional areas of individual astrocytes in culture and GFAP-positive cells in tissue slices were marked using the Histo tool in LSM 510 META or Zen software. The number of all pixels in marked areas, representing the total cell area, and the number of only red or green fluorescent pixels, representing Nile Red- or BODIPY^{493/503}-positive cell cross-sectional areas, respectively, were determined and the percentage of LD area per total cell area was calculated for individual experiments. The threshold intensity of the fluorescent signal was set to 20% of the maximum fluorescence intensity and was used to separate the background intensity from the fluorescent signal of Nile Red- or BODIPY^{493/503}-labelled pixels. In individual experiments, data were normalized to the average value of control untreated samples.

The number and perimeter of the LDs were determined in cross-sections of individual cells using Fiji software (Schindelin et al., 2012), Analyze Particles function after applying 20% threshold and signal intensity (watershed) segmentation on individual images. Then, assuming that all LDs are spherical, the LD diameter was estimated from the perimeter values with the equation $d = C/\pi$, where d is the diameter and C is the LD perimeter. In some experiments, LDs were counted manually and the LD diameter was measured as the full width at half maximum (FWHM) of the Gaussian curves fitted to the green fluorescence intensity profile in two perpendicular equatorial directions in Zen software. FWHM was measured only in LDs in focus.

To evaluate the LD area, perimeter, diameter, and number in the cortex of individual hemisphere of *Drosophila* brains, the cortical area of Nile Red-positive red pixels with fluorescence intensity above 35% of maximal fluorescence (Lipid droplet area) and total cortical area was determined for each stack of images separately in the brains from control flies and flies exposed to hypoxia and starvation using Fiji software (Schindelin et al., 2012). The values obtained were normalized to the average LD area per hemisphere in controls. The number of Nile Red-labelled LDs and LD perimeter per hemisphere were determined in each stack using Fiji, Analyze Particles function after applying 35% threshold. Then, assuming that all LDs are spherical, the LD diameter was estimated from the perimeter values with the equation $d = C/\pi$. The percentage of L10a-EGFP expressing glial cells associated with Nile Red-labelled LDs was determined in the brain cortex area manually by counting all cells and cells associated with LDs across individual

brain stack in control flies and flies exposed to hypoxia and starvation. The results obtained from brain stacks were averaged for the individual brain.

To evaluate the subcellular distribution of LDs in the soma and processes of the GFAP-stained astrocytes in brain tissue slices, LDs were counted manually and expressed as a percentage of LDs in soma or processes, respectively, per total LD number in a cell.

2.12 | Statistical analysis

Data are presented in bar charts (mean \pm SEM), distribution histograms, or box plots. Statistical significance between the groups was determined by Kruskal–Wallis one-way analysis of variance followed by Dunn's test, if not stated otherwise. $p < .05$ was considered significant. The number of independent experiments (n) and the number of analyzed cells is noted in figure legends.

3 | RESULTS

3.1 | Astroglial LDs are positioned near mitochondria and the ER

To identify LDs in astrocytes and to characterize their subcellular localization, we labeled intracellular organelles in isolated rat brain astrocytes immunocytochemically by transfection with GFP-organelle markers or with fluorescent dyes and quantified the extent of colocalization of fluorescently labeled LDs and organelle markers (Figure 1 and Figure S1).

Nile Red-labelled LDs highly colocalized with the LD-associated protein perilipin-2 (60% \pm 3%) and the BODIPY^{493/503} dye (62% \pm 4%), indicating the presence of LDs in astrocytes (Falchi et al., 2013; Farmer, Kluemper, & Johnson, 2019; Ioannou et al., 2019). The majority of LDs were positioned near mitochondria and/or ER. Consistent with this the degree of colocalization between Nile Red-labelled LDs and mitochondria (MitoTracker) or ER (Sec61 β) was relatively high (31% \pm 3% and 38% \pm 4%, respectively; highlighted in Figure 1a, insets) as observed in other cell types (Brasaemle & Wolins, 2012; Pu et al., 2011; Robenek et al., 2006; Shaw, Jones, & Wagenmakers, 2008). Gaussian curves were fitted to the frequency distribution plot of the distances between LDs to the nearest mitochondria, which were obtained by SIM microscopy and measurements of the distance between peaks of red (mitochondria) and green (LDs) fluorescence intensity profiles, revealed the value of 276 \pm 14 nm, which is smaller than the mean LD diameter of ~450 nm, suggesting that the majority of LDs are in close proximity, if not in contact with mitochondria (note that the distance between LDs and mitochondria depends on the LD diameter; Figure 1c). Further ultrastructural analysis of astrocytes using transmission electron microscopy (TEM) confirmed localization of LDs to the vicinity of mitochondria and the endoplasmic reticulum (ER; Figure 1d). The degree of colocalization of Nile Red-labelled LDs with secretory

vesicles (including small synaptic-like vesicles [SSLVs; D-serine, vGLUT1], peptidergic vesicles [ANP], lysosomes [LAMP1]), autophagosomes (in control [LC3] and glucose-deprived astrocytes [LC3 starvation]) and acidic vesicular compartments (LysoTracker) was low (<10%; Figure 1 and Figure S1), suggesting no major interaction of LDs with these organelles in astrocytes under basal conditions.

Thus, these data indicate that LDs in astrocytes are located near the mitochondria and the ER.

3.2 | Nutrient stress triggers accumulation of LDs in isolated and brain tissue astrocytes

To verify whether astrocytes accumulate LDs during nutrient stress, we exposed isolated cortical astrocytes and astrocytes in organotypic brain tissue slices for 24 hr to various nutrient stressors that are typically present during CNS pathologies (i.e., partial/complete nutrient deprivation, excess FFAs, and L-lactate). Cells were then fixed and labeled with LD markers (e.g., Nile Red or BODIPY^{493/503},

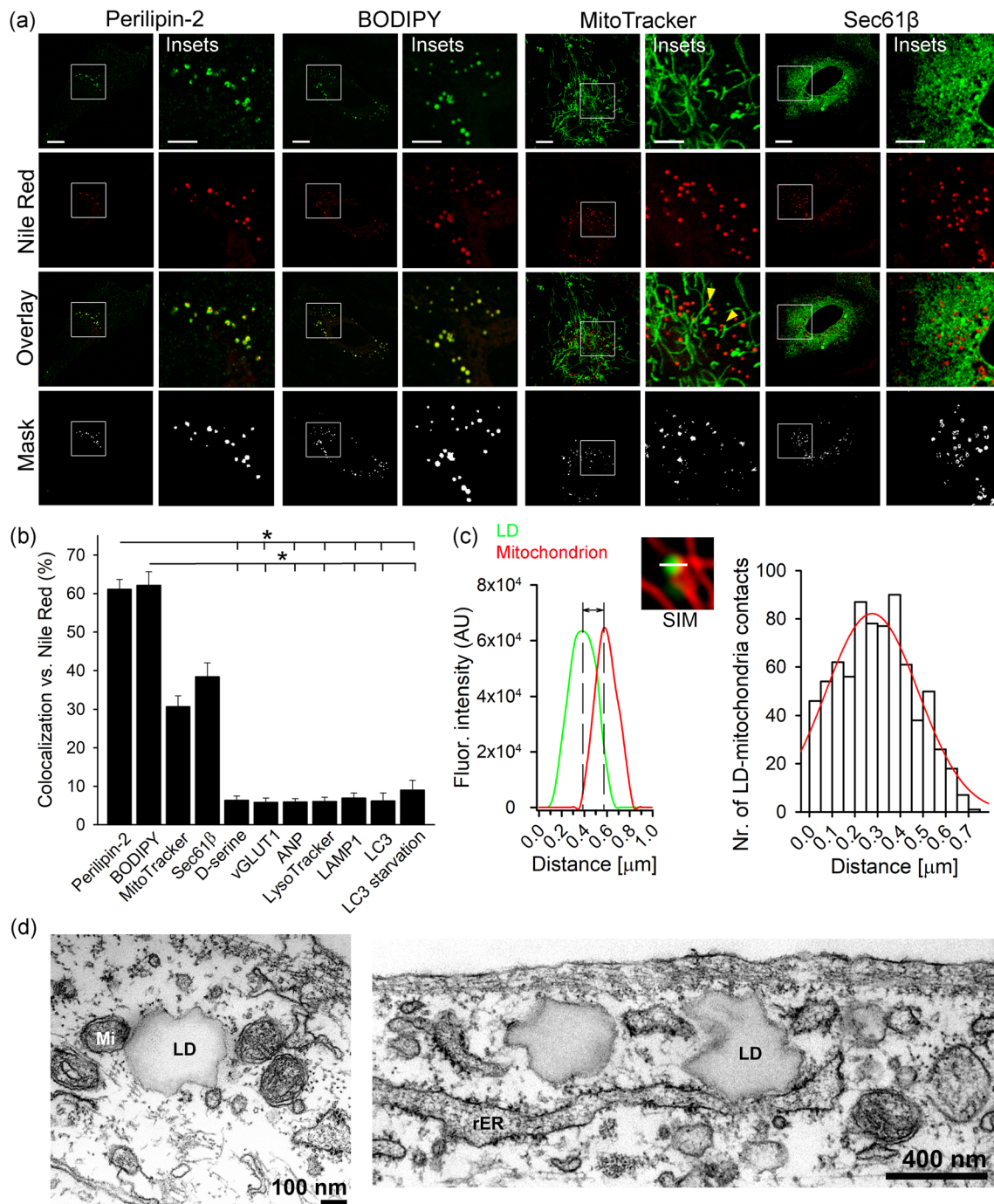


FIGURE 1 Legend on next page.

Figures 2 and 4). To identify astrocytes in brain tissue slices, the slices were immunostained with the astrocytic marker GFAP. Isolated and GFAP-positive tissue astrocytes were then imaged using confocal microscopy, and the content of LDs was determined in individual cells based on the Nile Red or BODIPY^{493/503} fluorescence pixel area and the number of Nile Red or BODIPY^{493/503} labeled LDs in an individual cell cross-sectional area.

Compared with control conditions (untreated cells in growth medium), partial (ECS with 10 mM glucose) nutrient deprivation caused a statistically significant increase in the Nile Red or BODIPY^{493/503} fluorescence pixel area per cell (LD area) in isolated astrocytes and astrocytes in brain tissue slices, respectively, both in cortical and hippocampal brain area ($p < .05$; Figures 2 and 4). Furthermore, complete (ECS without glucose) nutrient deprivation caused a statistically significant increase in LD area in isolated astrocytes ($p < .05$; Figure 2), and a trend in LD area increase in cortical and hippocampal astrocytes from brain tissue slices was observed (Figure 4). In addition to LD area, the cell LD number, and LD size (diameter and perimeter) increased in partially and completely nutrient-deprived isolated astrocytes compared to controls, respectively ($p < .05$, Figure 2c–e).

To study the effect of excess FFAs on LD accumulation in astrocytes, cells were exposed for 24 hr to 300 μ M OA. Upon exposure to OA, isolated astrocytes (Figure 2) as well as cortical and hippocampal astrocytes in brain tissue slices (Figure 4), exhibited increases in LD area, LD number, diameter, and perimeter compared with controls ($p < .05$).

To determine the effect of excess extracellular L-lactate concentration on LD accumulation in astrocytes, astrocytes were treated with 20 mM sodium L-lactate (L-lactate) for 24 hr. L-Lactate in cultured astrocytes triggered an increase in LD area (Figure 2b) and LD number (Figure 2c; $p < .05$), but not in LD size (diameter and perimeter) in comparison with controls. L-Lactate also increased the LD area per cell in cortical and hippocampal astrocytes (Figure 4b,c) from brain tissue slices compared with controls ($p < .05$). To verify that the addition of

20 mM sodium L-lactate into the growth medium did not affect LD accumulation in astrocytes by increasing solution osmolality, we performed control experiments replacing 20 mM sodium L-lactate with 40 mM D-sorbitol. The 40-mOsm increase in osmolality in the experiments with 40 mM D-sorbitol in the growth medium did not significantly affect LD area in either isolated or brain tissue astrocytes (Figures S2 and S3), indicating that the observed L-lactate-triggered increase in LD accumulation was not due to altered solution osmolality.

To determine the role of DGAT1 and DGAT2 enzymes that mediate the final step in TAG synthesis in LD biogenesis in astrocytes, isolated astrocytes were exposed to DGAT1 and DGAT2 inhibitors for 24 hr, which reduced the cell number and LD content by 40% and 75%, respectively ($p < .05$). DGAT1 and DGAT2 inhibitors also greatly reduced starvation-induced (i.e., complete nutrient deprivation) LD accumulation in astrocytes (Figure 3).

In conclusion, nutrient stress, including nutrient deprivation, excess of extracellular FFAs or lactate, triggers LD accumulation in isolated astrocytes and astrocytes in brain tissue. DGAT1 and DGAT2 enzymes are mediators of LD biogenesis in astrocytes in control conditions and under starvation.

3.3 | Hypoxia triggers accumulation of LDs in isolated astrocytes

To examine whether astrocytes accumulate LDs during hypoxic stress, we exposed isolated astrocytes and astrocytes in brain tissue slices to hypoxia (1% pO₂) for 24 hr. Cells and brain tissue slices were then fixed, labeled with LD markers (Figures 2 and 4), and in the case of tissue slices, the slices were immunostained with the astrocytic marker GFAP. Astrocytes were imaged by confocal microscopy and LD content was determined in individual cells. In comparison with controls, hypoxia increased LD area and LD number in cultured astrocytes

FIGURE 1 Subcellular colocalization of lipid droplets in isolated astrocytes. (a) Representative fluorescence images of isolated rat cortical astrocytes incubated in growth medium for 24 hr and labeled with fluorescent organelle markers (green) and Nile Red (red), a fluorescent marker for lipid droplets (LDs). Astrocytes were first labeled with antibodies against perilipin-2 (LD-binding protein; $n = 7$ [106 cells]), BODIPY^{493/503} dye (BODIPY; LD marker; $n = 9$ [99 cells]), MitoTracker dye (mitochondrial marker; $n = 16$ [86 cells]) or transfected with the plasmid pAc-GFPC1-Sec61beta (Sec61 β), to label the endoplasmic reticulum (ER marker; $n = 5$ [54 cells]; green, upper panels) and then stained with Nile Red. Merged images (Overlay) display colocalization (yellow) between the specific organelle markers (green) and Nile Red (red). Colocalization mask (Mask) between the green and the red fluorescence pixels. Insets show white boxed regions at higher magnification. Yellow arrows show the position of LDs near mitochondria. Representative images of astrocytes exposed to antibodies for D-serine ($n = 6$ [127 cells]) or the vesicular glutamate transporter 1 (vGLUT1; $n = 6$ [106 cells]) to label glutamatergic vesicles, peptidergic vesicles containing the atrial natriuretic peptide (ANP; $n = 5$ [101 cells]), acidic organelles, stained by the LysoTracker dye ($n = 18$ [103 cells]), lysosomes stained by antibodies against the lysosomal membrane protein 1 (LAMP1; $n = 9$ [99 cells]), autophagosomes stained by the antibodies against the light chain 3 (LC3; $n = 6$ [134 cells]) under normal and starvation conditions (LC3 starvation; $n = 6$ [123 cells]) are shown in Figure S1. Scale bars: 10 μ m and 5 μ m (insets). (b) Mean colocalization levels (%) of green fluorescent pixels (fluorescent organelle markers) compared with red fluorescent pixels (Nile Red, LDs). (c) Frequency distribution plot of the distances between LDs and mitochondria in control astrocytes. The distance between a LD to the nearest mitochondrion was determined by structured illumination microscopy (SIM) measuring the distance between the peaks of the BODIPY^{493/503} (green) and MitoTracker Red CMXRos (red) fluorescence intensity profiles in a single plane in 15 cells. The mean value for the distance between the LDs and the mitochondria, which was calculated by fitting a Gaussian curve on a frequency distribution plot, is 276 ± 14 nm. (d) Transmission electron micrographs of an astrocyte showing close proximity of LDs to mitochondria (Mi) and rough endoplasmic reticulum (rER). Bars represent means \pm SEM. n , number of independent experiments. * $p < .05$ (ANOVA, Dunn's test). Data for every set of experiments were obtained from at least three different animals [Color figure can be viewed at wileyonlinelibrary.com]

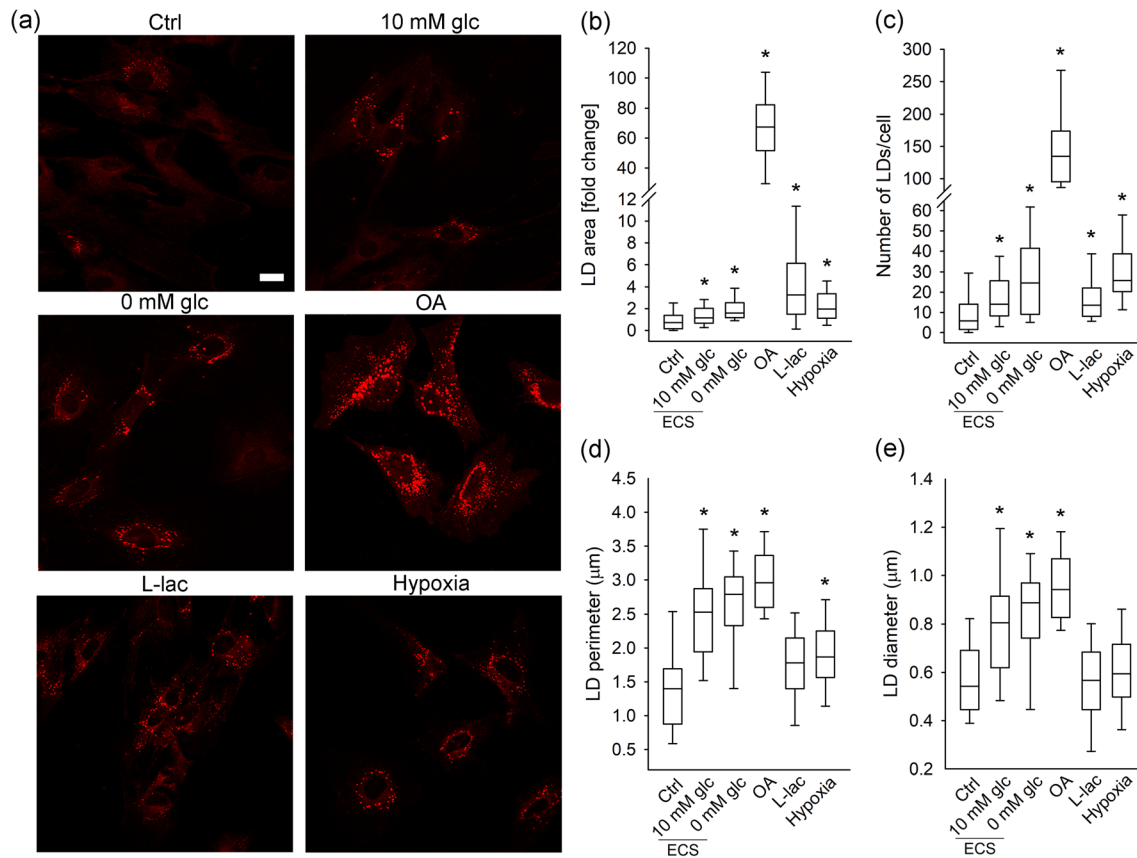


FIGURE 2 Lipid droplets in isolated astrocytes exposed to nutrient and hypoxic stress. (a) Representative fluorescence images of Nile Red-labelled isolated astrocytes incubated for 24 hr in growth medium (Ctrl; $n = 140$ [367 cells]), extracellular solution (ECS) with 10 mM glucose (10 mM glc; $n = 74$ [143 cells]) or without glucose (0 mM glc; $n = 81$ [157 cells]), and in growth medium (25 mM glc) with 300 μM oleic acid (OA; $n = 23$ [53 cells]), 20 mM L-lactate (L-lac; $n = 43$, [164 cells]), and under hypoxia (Hypoxia; $n = 53$ [139 cells]). Scale bar: 20 μm . (b–e) Box plots (center, median; box, IQR [interquartile range]; whiskers, 10th and 90th percentiles) of Nile Red-stained area per total cell area normalized to control (LD area [fold change]) (b), number of Nile Red-stained LDs per cell (c), and perimeter (d) and diameter of Nile Red-stained LDs (e) upon exposure of astrocytes to stress stimuli. LD perimeter and diameter were measured only in cells that contained LDs (n Ctrl = 107 [220 cells]; n 10 mM glc (ECS) = 43 [79 cells]; n 0 mM glc (ECS) = 42 [75 cells]; n OA = 24 [57 cells]; n L-lac = 39 [123 cells]; n Hypoxia = 57 [151 cells]). n , number of independent experiments. * $p < .05$ (ANOVA, Dunn's test). Data for every set of experiments were obtained from at least two different animals [Color figure can be viewed at wileyonlinelibrary.com]

($p < .05$; Figure 2b,c), but did not affect the LD area in astrocytes from brain tissue slices (Figure 4b,c).

3.4 | Exposure of *Drosophila melanogaster* to hypoxia and starvation triggers LD accumulation and increases the number of LD-associated glial cells in the fly brain

To investigate whether hypoxia and starvation affect accumulation of LDs in the CNS in vivo, we exposed adult *Drosophila* to hypoxia and starvation for 24 hr and stained isolated *Drosophila* brains with fluorescent LD marker Nile Red (Figure 5), while outlining glia through the expression of an EGFP under transcriptional control of the glia-specific repo (*repo-Gal4 > UAS-L10a-EGFP*).

First, we confirmed the presence of LDs in the *Drosophila* brain by co-staining brains isolated from wild-type flies (w^{1118}) with the LD markers Nile Red and BODIPY^{493/503} (Figure S7). Importantly, in flies

exposed to hypoxia and starvation (24 hr), the Nile Red-positive brain area, indicating LD content, and the number of LDs were significantly increased ($p < .05$; Figure 5b,c) compared to control flies raised on standard medium. Moreover, the mean proportion of EGFP-positive glial cells that contain or were in close contact with LDs (LD-associated Repo⁺ cells) was increased by 46% in the brains isolated from flies exposed to hypoxia and starvation compared to control flies ($p < .01$; Figure 5e).

These results show that in vivo hypoxic and nutrient stress conditions increase the accumulation of LDs in the brain.

3.5 | Noradrenaline triggers the accumulation of LDs

Noradrenergic signaling is greatly enhanced in the CNS during stress and, among many processes, also regulates brain metabolism, in particular, astroglial glucose energy metabolism and metabolic support of neurons (Dienel & Cruz, 2016; Dong et al., 2012; Kreft, Bak,

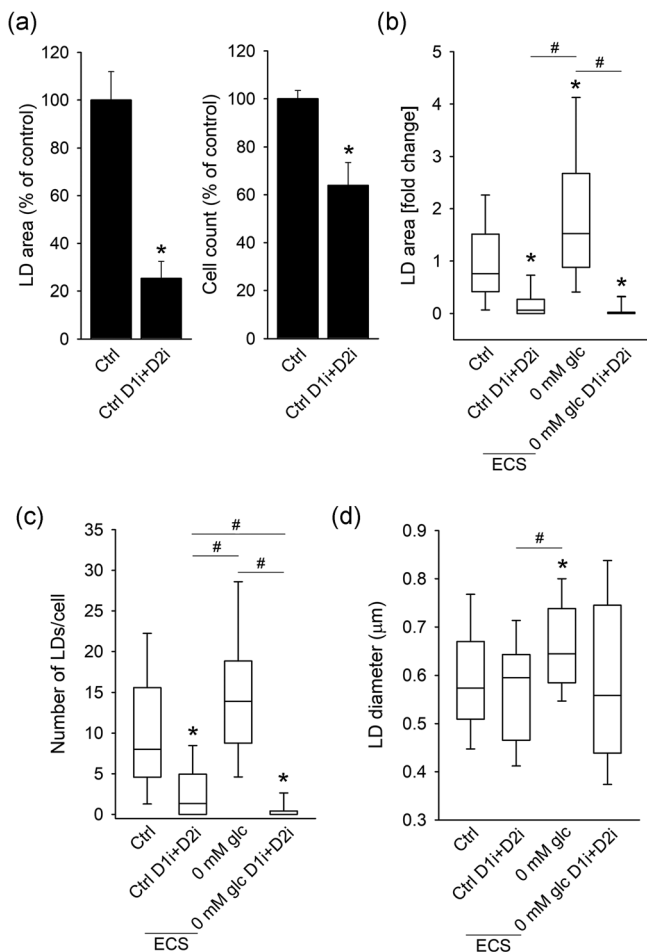


FIGURE 3 Inhibition of DGAT1 and DGAT2 enzymes in isolated astrocytes decreases cellular LD content and cell number. (a) Mean percentage of Nile Red-stained cell area per total cell area (LD area) and cell count in astrocytes incubated for 24 hr in growth medium (Ctrl; n for cell count = 7; n for LD area = 49 [281 cells]) or in growth medium upon simultaneous exposure to DGAT1 inhibitor (D1i; 10 μ M) and DGAT2 inhibitor (D2i; 10 μ M; Ctrl D1i + D2i; n for cell count = 7; n for LD area = 52 [253 cells]) expressed as % of control. (b–d) Box plots (center, median; box, IQR [interquartile range]; whiskers, 10th and 90th percentiles) of Nile Red-stained area per total cell area normalized to control (LD area [fold change]) (b), number of Nile Red-stained LDs per cell (c), and diameter of Nile Red-stained LDs (d) in astrocytes incubated for 24 hr in growth medium (Ctrl; n = 49 [281 cells]), growth medium in combination with DGAT1 and DGAT2 inhibitors (Ctrl D1i + D2i; n = 52 [253 cells]), extracellular solution (ECS) without glucose (0 mM glc; n = 54 [335 cells]) and extracellular solution without glucose in combination with DGAT1 and DGAT2 inhibitors (0 mM glc D1i + D2i; n = 52 [301 cells]). Diameter of LDs was measured only in cells that contained LDs (n Ctrl = 48 [196 cells]; n Ctrl D1i + D2i = 34 [105 cells]; n 0 mM glc (ECS) = 54 [282 cells]; n 0 mM glc (ECS) D1i + D2i = 20 [56 cells]). n , number of independent experiments. * p < .05 versus Ctrl (ANOVA, Dunn's test) and # p < .05 all pairwise (ANOVA, Dunn's test). Data for every set of experiments were obtained from three different animals

Waagepetersen, & Schousboe, 2012). To see whether it also affects astroglial LD dynamics, we exposed isolated and brain tissue astrocytes to NA (100 μ M; Figures 6 and 7). NA induced an increase in LD

area in isolated astrocytes (Figure 6) and in cortical and hippocampal astrocytes in brain tissue (Figure 7) compared with controls (p < .05). To see whether the observed increase in the LD area was due to an increase in LD number or size, we imaged astrocytes with SIM microscopy and determined the LD number per cell and the LD diameter as the FWHM fluorescence intensity (Figure 6d–f). NA caused a \sim 1.4-fold increase in LD diameter (0.434 ± 0.039 μ m [Ctrl, n = 6, 14 cells, 287 LDs] versus 0.618 ± 0.031 μ m [NA, n = 9, 13 cells, 498 LDs]; Figure 6d) and a \sim 2-fold increase in the number of LDs per cell (Figure 6e) compared with controls (p < .05). In the frequency distribution chart, the peak values for the LD diameter were 449 nm and 567 nm in control untreated and in NA-stimulated cells, respectively (Figure 6f). The results suggest that the number and the size of LDs increased upon noradrenergic activation, consistent with the accumulation of LDs in astrocytes.

3.6 | Noradrenaline triggers LD accumulation through activation of β - and α_2 -ARs in astrocytes

Given that adrenergic activation triggers LD accumulation in astrocytes, we further explored the contribution of selective activation of AR types (α_1 , α_2 , β_{1-3}) on LD accumulation. We exposed astrocytes for 24 hr to selective β -AR agonist isoprenaline (Iso, 100 μ M), α_1 -AR agonist phenylephrine (PE, 100 μ M), and α_2 -AR agonist dexmedetomidine (Dex, 50 nM).

Iso increased the LD area (Figure 6b) in isolated astrocytes and in astrocytes from the cortex and hippocampal area (Figure 7b, c) in brain tissue slices compared with control conditions (p < .05). Iso also increased the LD number in cortical and hippocampal astrocytes from brain tissue (Figure 7c). An increase in LD area was also observed upon Dex application in isolated astrocytes (Figure 6b) and in cortical and hippocampal (Figure 7b,c) astrocytes from brain tissue slices compared with controls (p < .05). Stimulation of astrocytes with PE caused only a small, insignificant increase in LD area compared with controls; in isolated astrocytes (Figure 6b) and in cortical and hippocampal astrocytes (Figure 7b,c).

Next, we analyzed the subcellular distribution of LDs in GFAP-stained astrocytes in brain tissue slices in control untreated cells and in cells treated with AR agonists. A significantly higher proportion of LDs in the cellular processes vs. somata was observed in control cortical astrocytes (p < .05; Figure 7e), while in control hippocampal astrocytes the proportion of LDs in processes vs. somata was similar. No considerable difference in subcellular LD distribution was observed in cortical or hippocampal astrocytes treated with NA (Figure 7e) or other AR agonists (Figure S8).

To further elucidate the role of individual AR types in LD accumulation in astrocytes, we pre-treated astrocytes with selective antagonists of ARs, Prop (β -AR), Atip (α_2 -AR), and Tera (α_1 -AR), and then exposed them to NA for 24 hr together with AR antagonists. We have observed that pretreatment with the selective β -AR antagonist Prop (1 μ M) reduced the NA-mediated increase in LD area in isolated astrocytes (p < .05; Figure 6c). Furthermore, Prop (10 μ M) reduced NA-mediated increase in cortical and hippocampal astrocytes in brain tissue slices (p < .05; Figure 7d). Pretreatment of isolated astrocytes

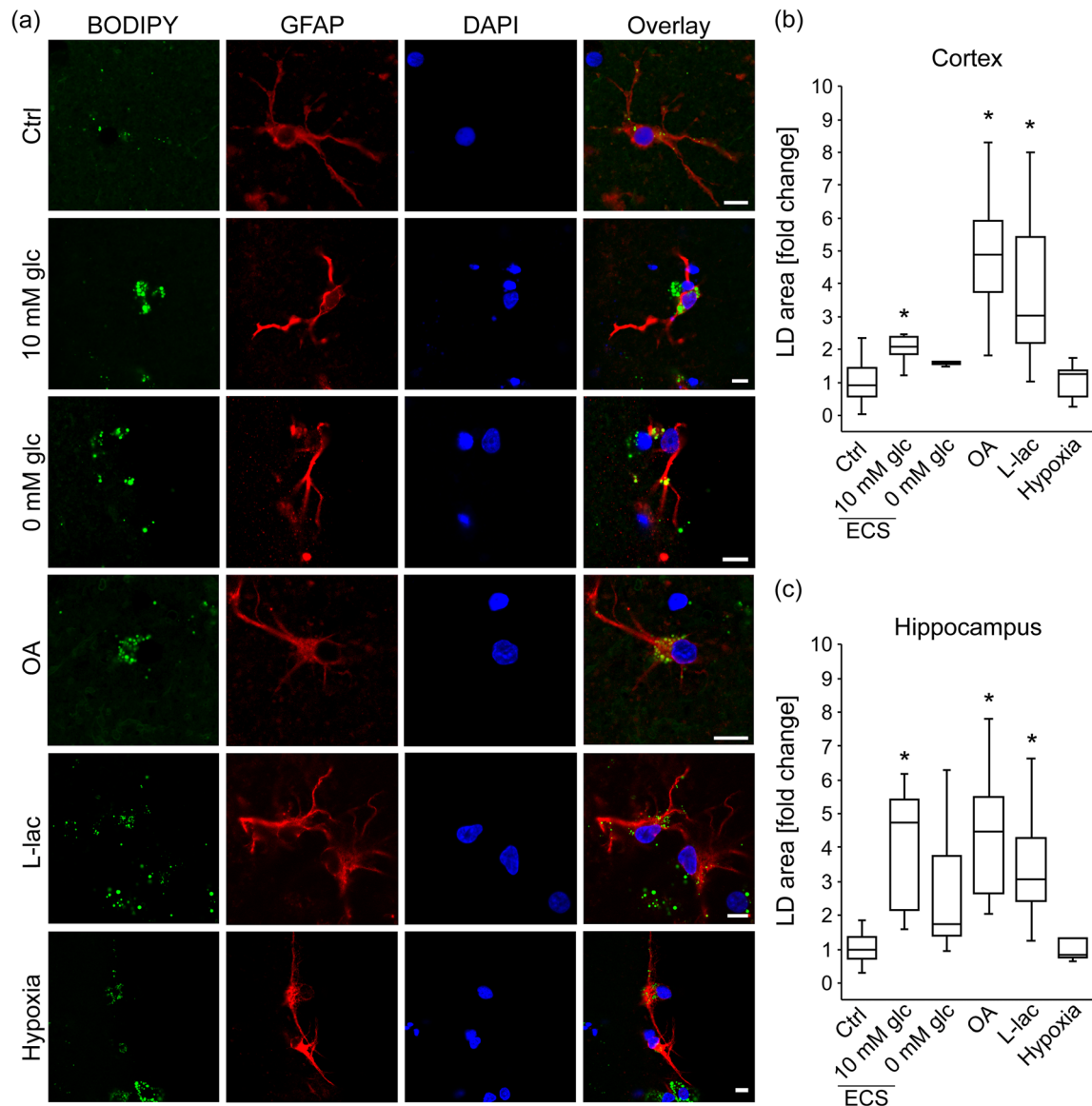


FIGURE 4 Lipid droplets in brain tissue astrocytes exposed to nutrient and hypoxic stress. (a) Representative fluorescence images of brain tissue astrocytes stained with BODIPY^{493/503} (BODIPY; green), antibodies against astrocyte-specific glial fibrillary acidic protein (GFAP; red) and nuclear marker 4',6-diamidino-2-phenylindole (DAPI; blue) incubated for 24 hr in growth medium (Control; Ctrl, 25 mM glucose; number for cortex [n_C] = 38 [358 cells]; number for hippocampus (n_H) = 23 [209 cells]), extracellular solution (ECS) with 10 mM glucose (10 mM glc; n_C = 6 [86 cells]; n_H = 7 [70 cells]) or without glucose (0 mM glc; n_C = 5 [88 cells]; n_H = 6 [63 cells]), and in growth medium with oleic acid (OA, 300 μ M; n_C = 13 [123 cells]; n_H = 9 [76 cells]), L-lactate (L-lac, 20 mM; n_C = 12 [95 cells]; n_H = 10 [69 cells]), and under 1% pO₂ (Hypoxia; n_C = 12 [105 cells]; n_H = 5 [65 cells]). Overlay represents merged images. Scale bars: 10 μ m. (b, c) Box plots (center, median; box, IQR [interquartile range]; whiskers, 10th and 90th percentiles) of BODIPY^{493/503}-stained area per total cell area normalized to control (LD area [fold change]) in astrocytes upon 24 hr treatment of brain tissue slices with various stress stimuli, separately for cortex (b) and hippocampus (c). n , number of independent experiments, * p < .05 (ANOVA, Dunn's test). Data for every set of experiments were obtained from at least two different animals [Color figure can be viewed at wileyonlinelibrary.com]

with Atip, a selective α_2 -AR antagonist, and Tera, a selective α_1 -AR antagonist, reduced the NA-mediated increase in LD area in isolated astrocytes (p < .05; Figure 6c), while Atip- and Tera-induced reduction in LD accumulation was insignificant in cortical and hippocampal astrocytes in brain tissue slices (Figure 7d). AR antagonists per se did not affect the LD area in astrocytes (Figures S4 and S5).

These results imply that the NA-triggered increase in LD accumulation in astrocytes is mediated via β - and α_2 -ARs.

3.7 | Mobility of LDs in isolated astrocytes is calcium-dependent and reduced under nutrient deprivation

To address the characteristics of LD mobility in astrocytes and to determine whether LD mobility is affected by nutrient stress, we monitored the mobility of Nile Red-labelled LDs in isolated astrocytes by real-time confocal microscopy in control and starved (24-hr

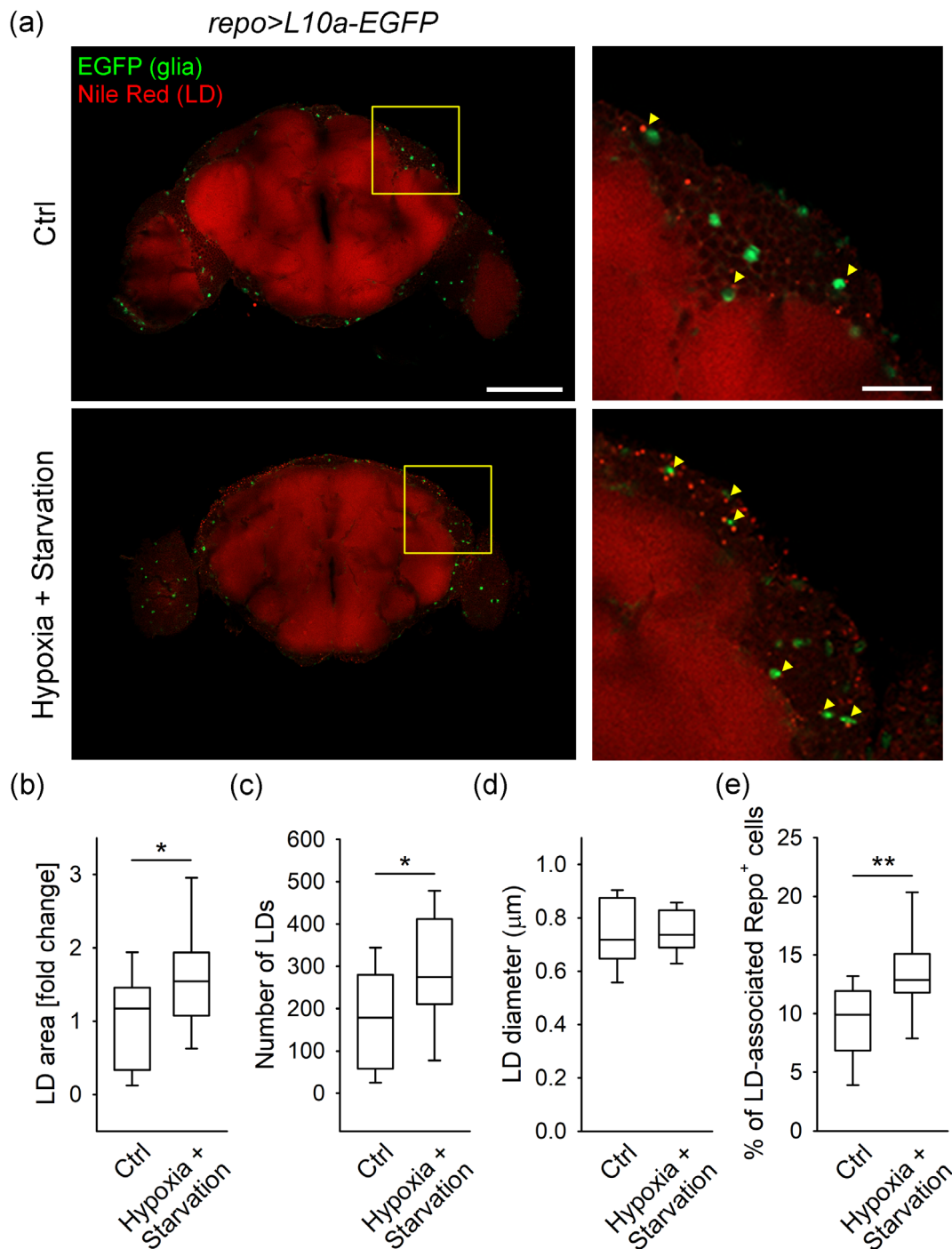


FIGURE 5 Hypoxia and starvation increases the LD content and the percentage of LD-associated glial cells in the *Drosophila* brain. (a) Representative fluorescence confocal images of adult *Drosophila* brains (left panels) labeled with lipid droplet (LD) marker Nile Red (red) and expressing L10a-EGFP in glial cells (using the *repo-Gal4* driver; green) isolated from control flies (Ctrl; $n = 12$, upper panel) and flies exposed to hypoxia and starvation (Hypoxia + Starvation; $n = 16$, lower panel). Right panels show yellow framed regions at higher magnification. Yellow arrowheads indicate cortical glial cells (green) associated with LDs (red). Shown are single optical sections, recorded by confocal microscope. Scale bars: 100 μm (left panels) and 20 μm (right panels). (b–e) Box plots (center, median; box, IQR [interquartile range]; whiskers, 10th and 90th percentiles) of Nile Red-labelled area per cortical brain area (LD area [fold change]) normalized to control (b), number of LDs (c), LD diameter (d) and percentage of LD-associated glial (Repo⁺) cells (e) in the brains from controls and flies exposed to hypoxia and starvation. Note that exposure of flies to hypoxia and starvation increases the brain LD area, LD number, and the proportion of glial (Repo⁺) cells associated with LDs. Only male flies were used. All experiments were performed under noncrowded conditions (<15 flies per vial) in duplicate. n , number of independent experiments, * $p < .05$, ** $p < .01$; Mann–Whitney Rank Sum Test (b and e) and Student's t -test (c) [Color figure can be viewed at wileyonlinelibrary.com]

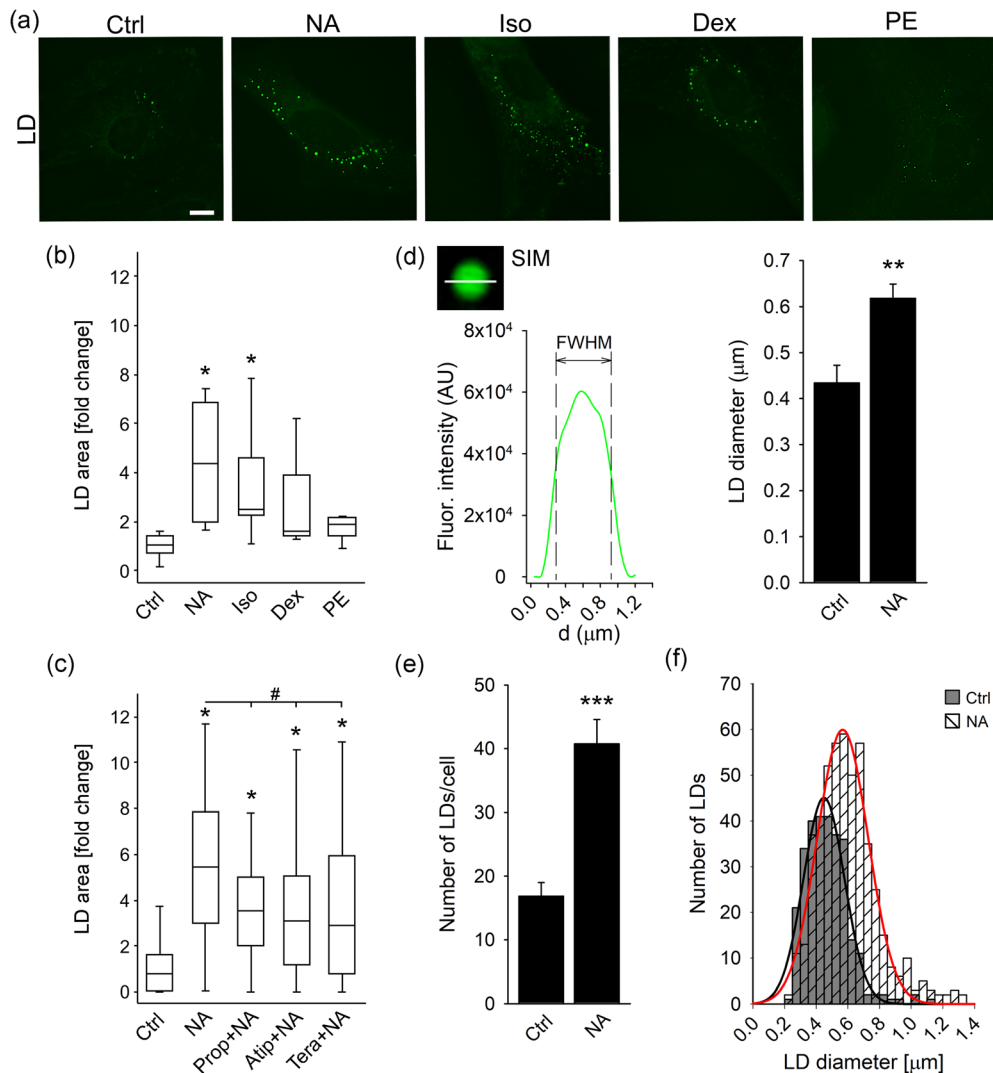


FIGURE 6 Noradrenaline increases the number and size of LDs in isolated astrocytes through activation of β -adrenergic receptors. (a) Representative fluorescence images of isolated astrocytes incubated for 24 hr in growth medium without (Control; $n = 6$ [113 cells]) and with various adrenergic receptor (AR) agonists, nonselective α -/ β -AR agonist noradrenaline (NA; 100 μ M; $n = 4$ [156 cells]), selective β -AR agonist isoprenaline (Iso; 100 μ M; $n = 5$ [114 cells]), selective α_2 -AR agonist dexmedetomidine (Dex; 50 nM; $n = 3$ [120 cells]), selective α_1 -AR agonist phenylephrine (PE; 100 μ M; $n = 4$ [126 cells]), and labelled with LD marker BODIPY^{493/503} (green). Scale bar: 10 μ m. (b, c) Box plots (center, median; box, IQR [interquartile range]; whiskers, 10th and 90th percentiles) of LD marker stained area per total cell area normalized to control (LD area [fold change]) in untreated astrocytes (Control; Ctrl) and in astrocytes exposed to (b) various AR agonists and (c) to NA (100 μ M; $n = 47$ [98 cells]) in the presence of various AR antagonists, β -AR antagonist propranolol (1 μ M; Prop + NA; $n = 54$ [121 cells]), α_2 -AR antagonist atipamezole (10 μ M; Atip + NA; $n = 57$ [124 cells]), and α_1 -AR antagonist terazosin (10 μ M; Tera + NA; $n = 56$ [136 cells]). (d, e) Mean LD diameter (d) and mean LD number per cell (e) in control untreated cells (Ctrl; n for LD diameter = 6 [14 cells] and n for LD number = 7 [73 cells]) and in cells exposed to NA (n for LD diameter = 9 [13 cells] and n for LD number = 11 [91 cells]) for 24 hr. The apparent LD diameter was determined by structured illumination microscopy measuring the full width at half maximum (FWHM) of the BODIPY^{493/503} fluorescence intensity profile in two perpendicular directions (only the horizontal direction is displayed; d, left panel). Bars represent means \pm SEM. n , number of independent experiments. * $p < .05$, ** $p < .01$, and *** $p < .001$ versus control and # $p < .05$ versus NA (ANOVA, Dunn's test (b and c) and Student's t -test (d and e)). (f) Frequency distribution of LD diameter in untreated controls (grey bars) and in cells treated with NA (striped bars) for 24 hr. Gaussian curves were fitted to LD diameter frequency distributions in untreated controls (black line; 287 analyzed LDs) and cells treated with NA (red line; 498 analyzed LDs). The mean peak values of the curves are 449 ± 8 nm in controls and 567 ± 7 nm in NA-treated cells. Data for every set of experiments were obtained from at least two different animals [Color figure can be viewed at wileyonlinelibrary.com]

exposure to ECS with 10 mM glucose) conditions before (i.e., spontaneous mobility) and after stimulation with 100 μ M ATP to increase intracellular Ca^{2+} levels (Bennett, Farnell, &

Gibson, 2005). Three parameters of LD mobility, TL, MD, and velocity, were determined for each condition, as described (Potokar et al., 2005).

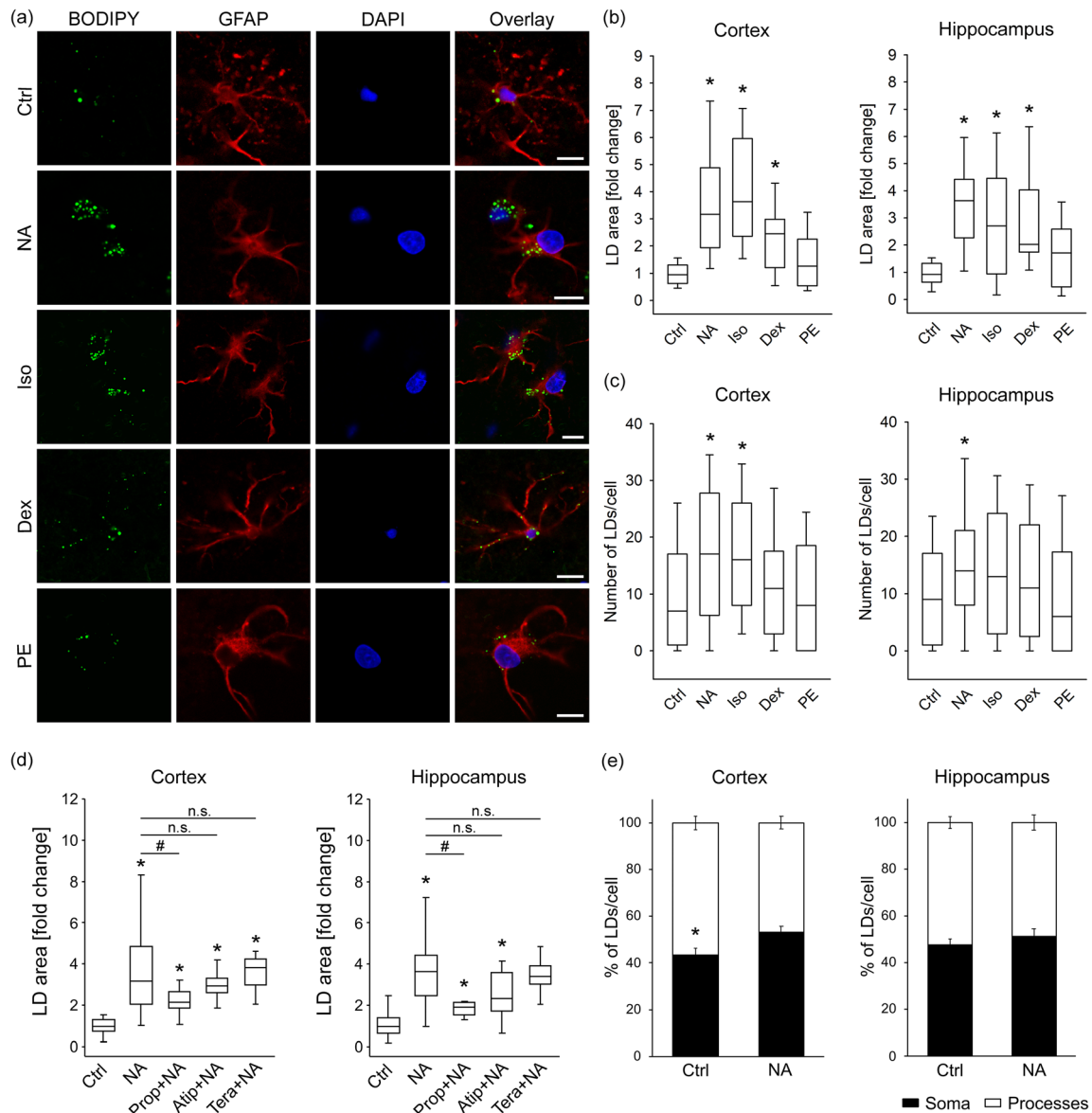


FIGURE 7 Noradrenaline-induced LD accumulation in brain tissue astrocytes through activation of β - and α_2 -adrenergic receptors. (a) Representative fluorescence images of brain tissue astrocytes stained with BODIPY^{493/503} (BODIPY; green), antibodies against astrocytic marker glial fibrillary acidic protein (GFAP, red), nuclear marker 4',6-diamidino-2-phenylindole (DAPI; blue), and merged images (Overlay) incubated for 24 hr in growth medium without (Control; Ctrl, 25 mM glucose; number for cortex (n_C) = 39 [403 cells]; number for hippocampus (n_H) = 38 [349 cells]) and with various adrenergic receptor (AR) agonists: nonselective α -/ β -AR agonist noradrenaline (NA; 100 μ M; n_C = 27 [242 cells]; n_H = 24 [164 cells]), selective β -AR agonist isoprenaline (Iso; 100 μ M; n_C = 12 [100 cells]; n_H = 13 [89 cells]), α_2 -AR agonist dexmedetomidine (Dex; 50 nM; n_C = 12 [99 cells]; n_H = 10 [79 cells]), and α_1 -AR agonist phenylephrine (PE; 100 μ M; n_C = 14 [105 cells]; n_H = 14 [124 cells]). Scale bars: 10 μ m. (b–d) Box plots (center, median; box, IQR [interquartile range]; whiskers, 10th and 90th percentiles) of BODIPY^{493/503}-stained area per total cell area normalized to control (LD area [fold change]) (b, d) and number of BODIPY^{493/503}-stained LDs per cell (c) in untreated control astrocytes (Ctrl) and (b, c) astrocytes exposed to various AR agonists and (d) NA (100 μ M) in combination with various AR selective antagonists (10 μ M); β -AR antagonist propranolol (Prop + NA; n_C = 12 [123 cells]; n_H = 10 [64 cells]), α_2 -AR antagonist atipamezole (Atip + NA; n_C = 11 [94 cells]; n_H = 10 [93 cells]), and α_1 -AR antagonist terazosin (Tera + NA; n_C = 12 [126 cells]; n_H = 8 [65 cells]), separately for cortical (Cortex) and hippocampal (Hippocampus) tissue astrocytes. (e) Mean percentage of BODIPY^{493/503}-stained LDs per cell soma (black bars) and processes (white bars) in untreated control astrocytes (Ctrl; n_C = 15 [111 cells]; n_H = 15 [114 cells]) and astrocytes exposed to NA (n_C = 10 [64 cells]; n_H = 8 [48 cells]), separately for cortical and hippocampal brain area. Bars represent means \pm SEM. n , number of independent experiments. * p < .05 versus Control and # p < .05 versus NA (ANOVA, Dunn's test (b–d)), * p < .05 all pairwise (ANOVA, Dunn's test (e)), n.s., not significant. Data for every set of experiments were obtained from at least two different animals [Color figure can be viewed at wileyonlinelibrary.com]

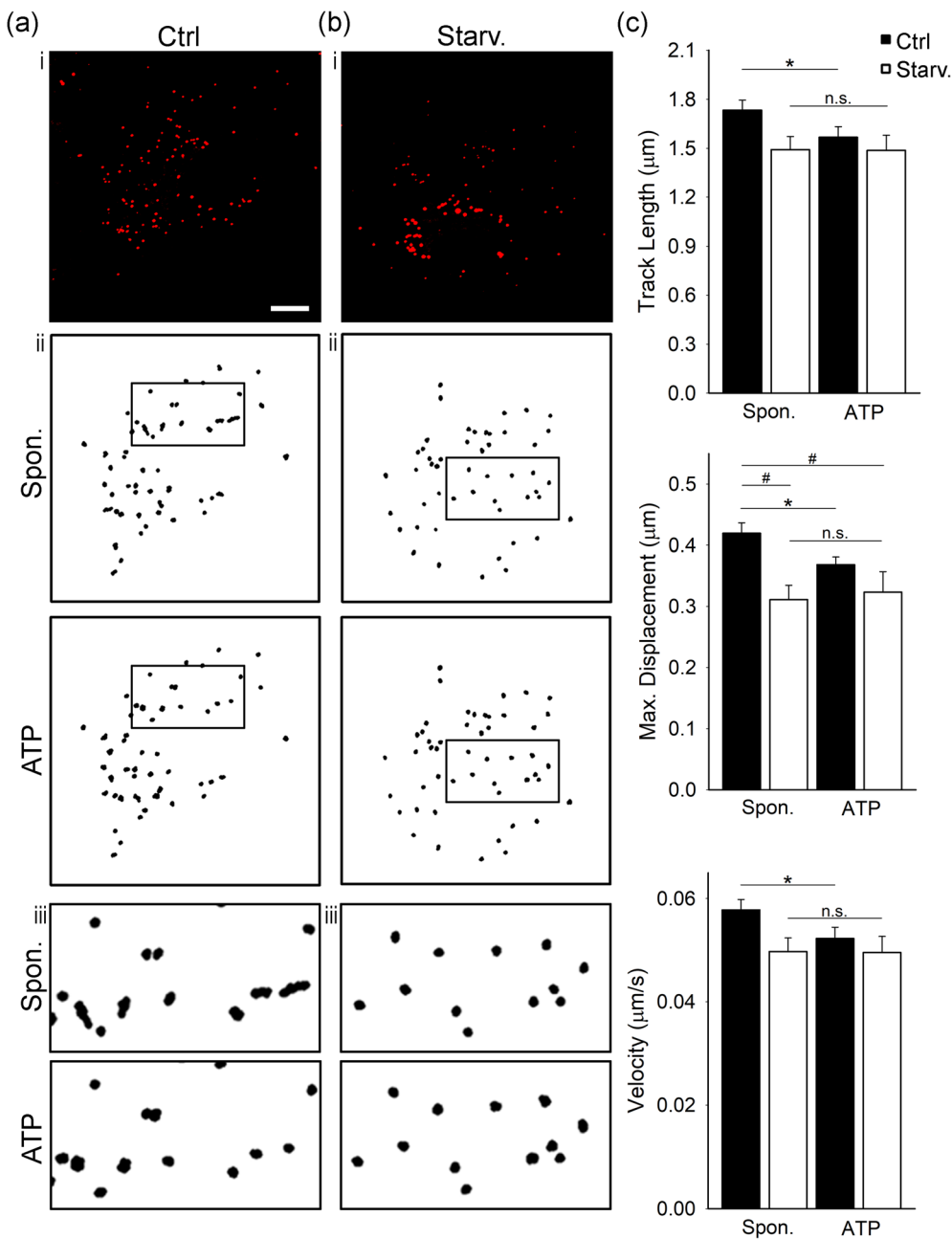


FIGURE 8 Mobility of LDs is reduced in glucose-deprived and ATP-stimulated isolated cortical astrocytes. (a-b, i) Representative fluorescence images of Nile Red-labelled isolated astrocytes incubated for 24 hr in (a, i) growth medium (Control; Ctrl, 25 mM glucose) and (b, i) under nutrient deprivation (10 mM glucose, Starv.). Red puncta represent fluorescently labeled lipid droplets (LDs). (a-b, ii and iii [insets]) Trajectories of 50 Nile Red-labelled LDs in a representative cell 60 s before (Spon.; upper panels) and 60 s after stimulation with ATP (ATP, 100 μM; lower panels in control (Ctrl) and under starvation (Starv.). Insets (iii) show black-boxed regions in (ii) at higher magnification. Scale bar: 10 μm. (c) Histograms of average LD track length, maximal displacement and velocity 60 s before (Spon.) and 60 s after the addition of ATP (ATP, 100 μM) in control (Ctrl; black bars; $n = 28$ [1,316 LDs]) and under nutrient deprivation (Starv.; white bars; $n = 8$ [514 LDs]). All mobility parameters were reduced by >10% under nutrient deprivation in spontaneous and in ATP-stimulated conditions. * $p < .05$ (paired *t*-test), # $p < .05$ (ANOVA, Dunn's test). Data for every set of experiments were obtained from at least two different animals [Color figure can be viewed at wileyonlinelibrary.com]

A reduction in the mobility of LDs was observed under starvation compared with controls; the mobility parameters were reduced: the MD was significantly reduced by 26% (0.41 ± 0.02 μm [control] versus 0.31 ± 0.02 μm [starvation]; $p < .05$), while the TL and velocity show a trend in reduction by 14% (1.73 ± 0.06 μm [$n = 28$, 1,316 LDs; control] versus 1.49 ± 0.08 μm [$n = 8$, 514 LDs; starvation]) and by 17% (0.06 ± 0.00 μm/s [control] versus 0.05 ± 0.00 μm/s [starvation]; Figure 8), respectively.

ATP stimulation, which increases cytosolic free Ca^{2+} concentration (Horvat, Zorec, & Vardjan, 2016), reduced the mobility of LDs in isolated astrocytes in control conditions. In control astrocytes, ATP stimulation triggered a 9% decrease in TL (1.73 ± 0.06 μm [spontaneous] versus 1.57 ± 0.07 μm [ATP]), a 12% decrease in MD (0.42 ± 0.02 μm [spontaneous] versus 0.37 ± 0.01 μm [ATP]) and a

17% decrease in velocity (0.06 ± 0.00 μm/s [spontaneous] versus 0.05 ± 0.00 μm/s [ATP]; $p < .05$). In starved astrocytes, the mobility parameters were unchanged upon ATP stimulation: TL (1.49 ± 0.08 μm [spontaneous] versus 1.49 ± 0.09 μm [ATP]), MD (0.31 ± 0.02 μm [spontaneous] versus 0.32 ± 0.03 μm [ATP]) and velocity (0.05 ± 0.00 μm/s [spontaneous] versus 0.05 ± 0.00 μm/s [ATP]; Figure 8).

Most of the LDs in control astrocytes exhibited a nondirectional type of mobility within 60 s of analysis with MD < 1 μm (Potokar et al., 2005). Only 48 of 1,316 LDs (3.65%) in spontaneous conditions and 24 of 1,316 LDs (1.82%) upon ATP stimulation exhibited directional mobility with MD > 1 μm. In starved cells, under spontaneous conditions and upon ATP stimulation, all LDs exhibited only non-directional mobility with MD < 1 μm (Figure S6).

These data indicate that LDs in resting astrocytes are relatively static organelles. Prolonged starvation and acute ATP stimulation reduce LD mobility, implying that the mobility of LDs in astrocytes is downregulated by intracellular Ca^{2+} increase and prolonged nutrient deprivation.

4 | DISCUSSION

During various brain pathologies, LDs were shown to accumulate in the human brain, predominantly in glia, and to a lesser extent in neurons. However, the LD biology and the mechanisms leading to LD accumulation in CNS pathologies are poorly understood. Here, we provide evidence that astroglial LDs are organelles of ~450 nm in diameter important for normal astrocyte function exhibiting primarily low mobility, confined to the proximity of mitochondria and ER. This mobility is further restrained by metabolic stress and stimulation of astrocytes. The exposure of astrocytes to NA, the neuromodulator of the stress response system in the CNS, and to metabolic and hypoxic stress facilitates the accumulation of LDs in astrocytes, increasing the number and the size of LDs. The nature of this change in astrocytes may be viewed as a support for energy provision but also to be neuroprotective against the stress-induced accumulation of FFAs and lipotoxicity.

4.1 | Astroglial LDs are important for normal cell function and exhibit limited mobility proximally to mitochondria and ER

LDs were recognized in some non-adipose cells not only as passive lipid storage organelles, providing substrates for energy metabolism and membrane synthesis, but also as dynamic, mobile organelles interacting with other intracellular compartments, that, depending on the cell type, can play a role in a number of additional cellular functions (Barbosa & Sinioglou, 2017; Kilwein & Welte, 2019; Olzmann & Carvalho, 2019; Thiam, Farese, & Walther, 2013). However, there is limited knowledge on the characteristics of LDs in astrocytes. We found that ~35% of isolated cortical astrocytes at basal conditions contain LDs of ~450 nm in diameter. When *de novo* biogenesis of LDs was attenuated by inhibition of DGAT1 and DGAT2 enzymes, the astrocyte cell number was reduced by ~40%, suggesting that LDs in astrocytes are important for the maintenance of cell cycle and/or cell survival.

LDs were typically clustered near the nucleus and located in the vicinity of (and may even directly associate with) mitochondria and ER as determined with SIM and TEM. This is consistent with previous studies in adipocytes (Blanchette-Mackie & Scow, 1983; Brasaemle & Wolins, 2012; Freyre, Rauher, Ejsing, & Klemm, 2019; Novikoff, Novikoff, Rosen, & Rubin, 1980), skeletal muscle cells (Shaw et al., 2008) and different cell lines (Herms et al., 2015; Rambold et al., 2015). In brain tissue slices, ~70% of astrocytes in basal conditions contained LDs, which were observed not only in soma but also inside astrocytic processes. In cortical astrocytes, the proportion of LDs was higher in processes than in soma, while in hippocampal

astrocytes, the distribution of LDs between processes and soma was similar. The LD-mitochondria contact sites may allow direct transport of FFAs from the LD core to the mitochondrial matrix for β -oxidation (Gao & Goodman, 2015; Herms et al., 2015; Pu et al., 2011; Rambold et al., 2015), whereas LD-ER contacts likely indicate sites of *de novo* biogenesis of LDs (Robenek et al., 2006; Walther & Farese, 2012). Besides their essential role in lipid oxidation, mitochondria may also provide building blocks, energy, and redox equivalents for *de novo* lipogenesis, triglyceride synthesis, and LD assembly within the ER (Benador, Veliova, Liesa, & Shirihai, 2019; Petan, 2020). Therefore, the interactions between mitochondria and LDs observed in astrocytes may also be anabolic in nature, a hypothesis that remains to be tested in future studies. In contrast to mitochondria and ER, LDs do not show any major colocalization with other astroglial cellular organelles tested, including SSLVs, peptidergic vesicles, and acidic compartments (e.g., lysosomes, autophagosomes).

LDs must exhibit a certain degree of mobility to ensure their interaction with other organelles. We provide evidence that LDs in astrocytes display limited mobility. In comparison with astroglial secretory vesicles, they exhibit one order of magnitude lower average velocity (~60 nm/s) with the exception of late endolysosomes, which exhibit limited mobility similar to LDs (Potokar, Stenovec, Kreft, Gabrijel, & Zorec, 2011). More than 95% of LDs jittered with an average velocity of ~60 nm/s in a confined area displaying MDs < 1 μm within the recording time of 1 min, suggesting motion around a tethered point at mitochondria or ER. Only a minority (<5%) of LDs exhibited directional, likely cytoskeleton-associated, mobility (Kilwein & Welte, 2019; Potokar et al., 2005), with MDs >1 μm and average velocity of ~110 nm/s. The relatively faster directional mobility might be important for the delivery of LDs to contact sites with other cellular organelles, such as mitochondria, ER, other LDs, with the mission to exchange lipids (Kilwein & Welte, 2019), or to the plasma membrane and subsequent extrusion from astrocytes (Falchi et al., 2013). However, we have not observed any LD-plasma membrane fusion events during our recording time. Prolonged starvation and stimulation of astrocytes with ATP, which mobilizes intracellular Ca^{2+} in astrocytes (Bennett et al., 2005; North & Verkhratsky, 2006), attenuates LD mobility in astrocytes. Such reduction in LD mobility could strengthen the connection between LDs and mitochondria or ER, enhancing the transport of lipids from the LDs to cellular organelles and vice versa during times of starvation or stimulation.

4.2 | Astrocytes accumulate LDs in response to metabolic and hypoxic stress

Astrocytes are crucial for the homeostatic regulation of CNS metabolism. They uptake energy substrates, such as glucose and FFAs, from the blood circulation and can store them in the form of glycogen (Bak, Walls, Schousboe, & Waagepetersen, 2018) and, under conditions related to CNS pathologies, in LDs (Barber & Raben, 2019). In contrast, neurons are not energy-storing cells and do not normally contain glycogen (Barros, 2013) or LDs (Barber & Raben, 2019). Compared to



glycogen, the role of astroglial LDs in the CNS is much less studied. Environmental nutrient and hypoxic stress have been linked to the formation of LDs in some non-adipocyte cell types (Henne et al., 2018) and might also trigger LD accumulation in glial cells when nutrient and oxygen supplies in diseased CNS regions are limited, completely depleted, or even in excess.

We show here that exposure of astrocytes in pure cultures and brain tissue slices to nutrient deprivation facilitates accumulation of LDs, increasing the number and the size of LDs. Most likely, astrocytes under starvation convert their own structural components of membranes into energy-rich FFAs and use them as an alternative energy source in mitochondrial β -oxidation. However, to prevent cytotoxic effects of the released FFAs, they first esterify FFAs into energy-rich molecules (TAGs) and pack them into LDs (Farmer et al., 2019; Nakajima, Gotoh, Fukasawa, Murakami-Murofushi, & Kunugi, 2019; Nguyen et al., 2017; Rambold et al., 2015). Consistent with this, we show here that selective inhibition of DGAT1 and DGAT2, enzymes responsible for the final steps of TAG synthesis, was sufficient to prevent starvation-induced LD biogenesis in isolated astrocytes. In the brain tissue, besides endogenous lipids, the external lipids derived from other cell types may also represent a lipid source for LD formation in astrocytes. Consistent with the astroglial capacity to store FFAs in LDs, isolated astrocytes (Kis et al., 2015; Nakajima et al., 2019) and brain tissue astrocytes exposed to an excess of extracellular FFAs (OA) accumulate LDs. FFAs can be mobilized from LDs for mitochondrial β -oxidation either by cytosolic lipases (Chaves, Frasson, & Kawashita, 2011; Etschmaier et al., 2011; Zechner, Madeo, & Kratky, 2017) or by autophagosomal degradation of LDs (K. Liu & Czaja, 2013; Ouimet et al., 2011; R. Singh et al., 2009). Starvation for 24 hr to induce autophagy did not trigger any increase in the content of the autophagosomal marker LC3 (data not shown), however, the extent of colocalization between the LDs and the autophagosomal marker LC3 in astrocytes exposed to 24 hr starvation was increased by 30%, suggesting a potential association of some LDs with autophagosomes during starvation (Rambold et al., 2015). During states of hypoglycemia, by accumulating LDs, astrocytes might switch from glucose to lipid metabolism, which can increase astroglial viability in times of prolonged glucose deprivation, as observed in a glioma LN18 cell line (Cabodevilla et al., 2013). This way they spare any remaining glucose for neuronal metabolism, because FFAs can be used as a fuel mostly by glial cells, whereas neurons are too vulnerable to ROS generated during β -oxidation (Bruce et al., 2017; Panov, Orynbayeva, Vavilin, & Lyakhovich, 2014; Schonfeld & Reiser, 2013). Given that astrocytes are ketogenic cells, FFAs from astroglial LDs might also be converted under brain tissue starvation into ketone bodies, which can be transported to neurons as an alternative source of energy (Guzmán & Blázquez, 2001, 2004), increasing neuronal viability. This needs to be further examined.

Most CNS pathologies, including ischemia, injury, cancer, and neurodegeneration, are associated not only with hypoglycemia but also with hypoxia (X. Guo, Namekata, Kimura, Harada, & Harada, 2017; Kawabori & Yenari, 2015; Laurenti et al., 2011; Petan, 2020; Petan et al., 2018; Zoula et al., 2003), favoring anaerobic

metabolism with glycolytic production of L-lactate, which exits neural cells and may accumulate in extracellular space, causing hyperlactatemia (Proia, Di Liegro, Schiera, Fricano, & Di Liegro, 2016). The physiological concentration of extracellular L-lactate in the brain (~0.1–1.4 mM) can increase to ≥ 10 mM in the above-mentioned pathologies (Mosienko et al., 2015), which could also affect the astroglial LD metabolism. Exposure of isolated and brain tissue astrocytes for 24 hr to an increased extracellular L-lactate concentration (20 mM) under normoxic and normoglycemic conditions facilitated LD accumulation. Exogenous L-lactate may enter astrocytes through lactate monocarboxylate transporters and lactate channels (Sotelo-Hitschfeld et al., 2015), to be used as a metabolic substrate for de novo FFA synthesis, as shown in oligodendrocytes (Sanchez-Abarca, Taberero, & Medina, 2001) and neurons, where lactate is decarboxylated in mitochondria and the resulting acetyl-CoA generates FFAs (Ioannou et al., 2019; L. Liu et al., 2017). This could trigger LD accumulation to protect astrocytes from FFA overload and lipotoxicity (Bailey et al., 2015; Ioannou et al., 2019; L. Liu et al., 2017; L. Liu et al., 2015). In tissue slices, it is also possible that L-lactate enters neurons first, where it is transformed to FFAs and subsequently transported to astrocytes. This was addressed in recent studies demonstrating that astroglial L-lactate entering neurons via ANLS is the driving force for FFA production in stressed overstimulated neurons. Lactate-derived FFAs are then transported from neurons to astrocytes in vesicles containing apolipoprotein E-like particles and stored in astroglial LDs, because astrocytes, in contrast to neurons, have the capacity to use FFAs in β -oxidation and fight the mitochondrial overproduction of ROS during β -oxidation (Bailey et al., 2015; Ioannou et al., 2019; L. Liu et al., 2017; L. Liu et al., 2015). Moreover, increased extracellular L-lactate concentrations may also activate cell surface G-protein coupled receptor 81 (half-maximal effective concentration ≈ 5 mM; C. Liu et al., 2009), located on the surface of brain cells (Lauritzen et al., 2014; Morland et al., 2015), as in adipocytes (Ahmed et al., 2010; C. Liu et al., 2009). This may downregulate the formation of cytosolic cAMP, thus inhibiting the activity of cAMP-dependent lipolytic enzymes and lipolysis, promoting energy storage in LDs, as observed in myotubes (Sun, Ye, Xie, & Ye, 2016).

Moreover, our studies demonstrate that hypoxic stress, a common etiology of various CNS diseases, induced by hypoxia (1% O₂ for 24 hr) in normoglycemic conditions triggers LD accumulation in isolated astrocytes. Astroglial LD accumulation may be induced by a potentiation of glycolytic lactate production under hypoxia, which can in turn trigger FFA production from L-lactate and storage of excess FFAs in astroglial LDs, as discussed. Hypoxia also triggers increased ROS production (Islam et al., 2019). If the ROS production is much higher than the cellular antioxidant capacity, it can induce peroxidation of membrane lipids (also proteins and nucleic acids), particularly polyunsaturated fatty acids, both in astrocytes and neurons. Under oxidative stress, polyunsaturated fatty acids were shown to be transferred from cell membranes to the glial LD core, where they are less vulnerable for lipid peroxidation chain reaction (Bailey et al., 2015). Consistent with this, cultured astrocytes with LDs were shown not only to upregulate genes to neutralize ROS but also genes involved in

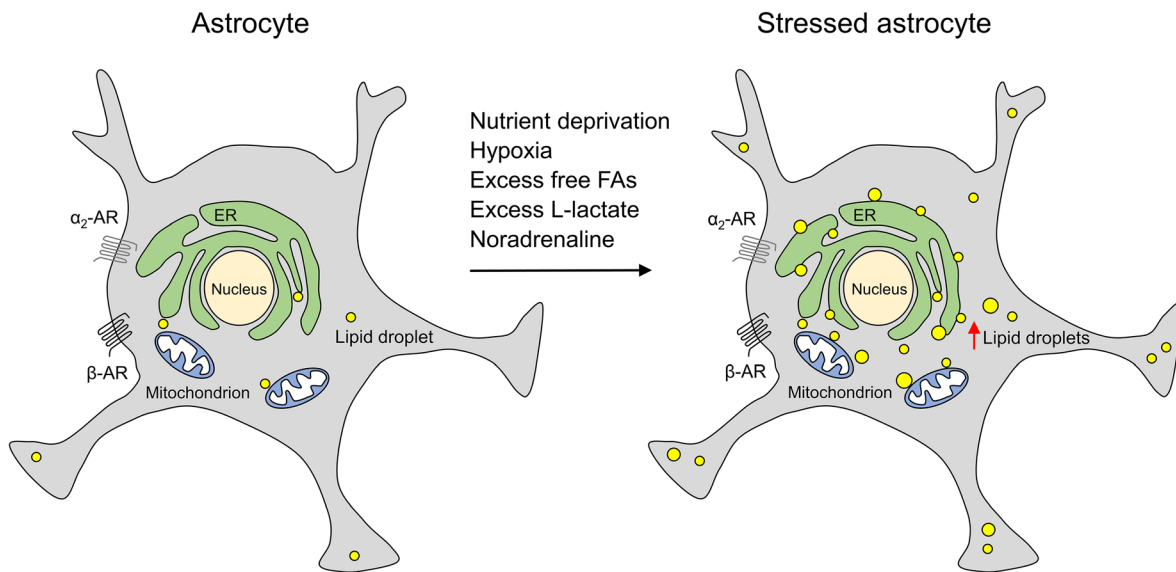


FIGURE 9 Stressed astrocytes accumulate LDs. LDs in astrocytes are organelles with limited mobility positioned in close proximity to mitochondria and ER most likely to enable a stronger interaction between these organelles and thus more efficient β -oxidation and LD biogenesis, respectively. Noradrenaline, a brain stress-response system neuromodulator, metabolic stress (nutrient deprivation, excess of free FAs, and L-lactate), and hypoxic stress strongly increase LD accumulation in astrocytes by increasing the number and the size of LDs. Noradrenaline increases LD accumulation through activation of β - and α_2 -ARs. Accumulation of LDs in stressed astrocytes may be viewed as a support for energy provision, but may also provide neuroprotection against the stress-induced lipotoxicity. AR, adrenergic receptor; ER, endoplasmic reticulum; FAs, fatty acids; LD, lipid droplet [Color figure can be viewed at wileyonlinelibrary.com]

FFA transport and metabolism, likely promoting accumulation of LDs and β -oxidation (Ioannou et al., 2019). Fatty acid-binding protein 7 was recently proposed to protect isolated astrocytes exposed to a combination of chronic hypoxia and hypoglycemia from ROS toxicity by LD formation (Islam et al., 2019). Moreover, chronic hypoxia can trigger activation of the HIF-1 and HIF-2 pathways in astrocytes (M. Guo et al., 2019), which may activate transcription factors altering the expression pattern of proteins involved in lipid transport and lipid metabolism, favoring LD accumulation in astrocytes, as observed in other cell types (Furuta et al., 2008; Krishnan et al., 2009; Sekiya, Hiraishi, Touyama, & Sakamoto, 2008).

Moreover, hypoxia and starvation triggered accumulation of LDs in the *Drosophila* brain, indicating that the systemic response to hypoxic and nutrient stressors involves accumulation of LDs in the brain in vivo. LDs were observed to associate with glial cells, which is consistent with results obtained from the larval *Drosophila* brain (Bailey et al., 2015; Kis et al., 2015), implying involvement of glial cells in the LD metabolism in adult *Drosophila* brain. During extreme conditions, where the energy demands are increased, *Drosophila* energy provision largely depends on the fat body (functional equivalent to mammalian adipose tissue and liver), the major lipid storage site. The lipids stored in the fat body may be transported to target sites under stress (Toprak, Hegedus, Doğan, & Güney, 2020), including the brain. Thus, upon hypoxia and starvation flies may utilize fat sources from the fat body or other organs for LD accumulation in the brain (Henne et al., 2018; Schulz et al., 2015).

Taken together, these data indicate that although glial LD accumulation has been associated with neuronal signals, we show here

that not only tissue-associated astrocytes, but also isolated astrocytes cut off from neural signals possess mechanisms to respond to prolonged nutrient and hypoxic stress with LD accumulation. Accumulation of LDs may help stressed astrocytes to resist FFA overload and lipotoxicity and to promote energy metabolism. All of which may also contribute and augment neural cell viability during CNS pathologies.

4.3 | Stress-related noradrenergic activation triggers LD accumulation in astrocytes via β - and α_2 -ARs

Astrocytes express all types of ARs and may respond to activation of the stress response *locus coeruleus*-noradrenergic system, which releases NA, with changes in intracellular Ca^{2+} and cAMP levels, affecting many aspects of astrocyte physiology, including glucose metabolism (Bélanger et al., 2011; O'Donnell, Zeppenfeld, McConnell, Pena, & Nedergaard, 2012). Here, we show for the first time that NA also affects astroglial LD metabolism. Long-term exposure (24 hr) of isolated and brain tissue astrocytes to NA leads to LD accumulation by increasing the number and the size of LDs. LD accumulation was mediated via activation of β - and α_2 -ARs, whereas activation of α_1 -ARs did not significantly affect it. These findings are consistent with the results in adipocytes, where α_1 -AR/ Ca^{2+} signaling is not involved in the regulation of lipid metabolism (Duncan, Ahmadian, Jaworski, Sarkadi-Nagy, & Sul, 2007), whereas α_2 -AR-mediated down-regulation of cAMP synthesis inhibits lipolysis and promotes LD accumulation (Chaves et al., 2011). Surprisingly, in contrast to our results



on astrocytes, where the prolonged activation of β -ARs triggers LD accumulation, in other cell types, including adipocytes (Chaves et al., 2011), hepatocytes (Schott et al., 2017), and myocytes (Morales, Bucarey, & Espinosa, 2017), activation of the β -AR/cAMP pathway promotes lipolysis by activating cAMP-dependent protein kinase A, which phosphorylates adipose triglyceride lipase, hormone-sensitive lipase, and perilipin-1, causing LD degradation. β -AR/cAMP activation in astrocytes could trigger metabolic (Dienel & Cruz, 2016) and transcriptional responses (Pardo et al., 2017). It upregulates glycogenolysis, aerobic glycolysis, and lactate production in astrocytes (Dienel & Cruz, 2016; Vardjan et al., 2018) and accumulated L-lactate could trigger de novo synthesis of FFAs and storage of FFAs in astroglial LDs (L. Liu et al., 2017). β -AR activation also activates transcriptional factor cAMP-response element-binding protein (CREB), which upregulates transcription of some genes involved in lipid metabolism in astrocytes, but not in neurons (Pardo et al., 2017), and may promote LD accumulation selectively in astrocytes. Interestingly, besides LD accumulation, long-term noradrenergic activation also triggers upregulation of glycogen synthesis in astrocytes via β -AR and CREB-dependent gene transcription as well as via acute α_2 -AR stimulation (Hertz, Chen, Gibbs, Zang, & Peng, 2004), suggesting that β - and α_2 -AR signaling are involved in noradrenergic upregulation of both glucose (i.e., glycogen) and lipid storage (i.e., LDs) mechanisms in astrocytes.

5 | CONCLUSIONS

We show here that LDs in astrocytes are organelles of ~450 nm in diameter, positioned in the soma and inside astrocytic processes in close proximity to mitochondria and ER. They exhibit limited but regulated mobility. Upon starvation and stimulation, LD mobility is decreased, likely enabling a stronger connection between LDs and mitochondria or ER for efficient β -oxidation or LD biogenesis, respectively. Stress-related noradrenergic activation and metabolic/hypoxic stress facilitate LD accumulation in isolated astrocytes in the absence of neuronal signals and in brain tissue astrocytes, increasing the number and the size of LDs (Figure 9). These may promote FFA energy metabolism in stressed astrocytes and protect neural cells from stress-induced overload of lipids and lipotoxicity in brain pathologies.

ACKNOWLEDGEMENTS

The authors thank Miha Pate, Primož Runovc, Erik Janežič, and Rhea Teng for support with the experiments. The authors' work was supported by grants from the Slovenian Research Agency (P3-0310, J3-2523, BI-DE/18-19-015, J3-9266, J7-2594, P1-0207, J7-1818), grants from the German Research Foundation (FOR 2149/P01, SCHO 1791/1-2, CRC1423/B06, DFG, EXC-1003) and COST Actions CM1207 (GLISTEN), CA18133 (ERNEST), CA19105 (EpiLipidNET).

CONFLICT OF INTEREST

The authors declare no competing financial interests.

AUTHOR CONTRIBUTIONS

Tina Smolič, Anemari Horvat, Urška Černe performed experiments, analyzed data, prepared figures, and wrote the manuscript. Petra Tavčar performed experiments, analyzed data, and prepared figures. Ana Halužan Vasle performed experiments and analyzed data. Mateja Erdani Kreft and Larisa Tratnjek performed EM, analyzed data, and prepared figures. Nicole Scholz and Maja Matis co-assisted with *Drosophila* experiments. Toni Petan co-assisted with the original idea of the manuscript. Robert Zorec co-wrote the manuscript. Nina Vardjan designed and directed the study, analyzed data, prepared figures, and wrote the manuscript.

DATA AVAILABILITY STATEMENT

All data generated or analysed during this study are included in this published article and its Supplementary Information files or are available from the corresponding author on reasonable request.

ORCID

Robert Zorec  <https://orcid.org/0000-0002-7478-3875>

Nina Vardjan  <https://orcid.org/0000-0001-8174-1668>

REFERENCES

- Ahmed, K., Tunaru, S., Tang, C., Müller, M., Gille, A., Sassmann, A., ... Offermanns, S. (2010). An autocrine lactate loop mediates insulin-dependent inhibition of lipolysis through GPR81. *Cell Metabolism*, 11(4), 311–319. <https://doi.org/10.1016/j.cmet.2010.02.012>
- Bailey, A. P., Koster, G., Guillemier, C., Hirst, E. M., MacRae, J. I., Lechene, C. P., ... Gould, A. P. (2015). Antioxidant role for lipid droplets in a stem cell niche of *Drosophila*. *Cell*, 163(2), 340–353. <https://doi.org/10.1016/j.cell.2015.09.020>
- Bak, L. K., Walls, A. B., Schousboe, A., & Waagepetersen, H. S. (2018). Astrocytic glycogen metabolism in the healthy and diseased brain. *The Journal of Biological Chemistry*, 293(19), 7108–7116. <https://doi.org/10.1074/jbc.R117.803239>
- Barba, I., Cabañas, M. E., & Arús, C. (1999). The relationship between nuclear magnetic resonance-visible lipids, lipid droplets, and cell proliferation in cultured C6 cells. *Cancer Research*, 59(8), 1861–1868.
- Barber, C. N., & Raben, D. M. (2019). Lipid metabolism crosstalk in the brain: Glia and neurons. *Frontiers in Cellular Neuroscience*, 13, 212–212. <https://doi.org/10.3389/fncel.2019.00212>
- Barbosa, A. D., & Siniouoglou, S. (2017). Function of lipid droplet-organelle interactions in lipid homeostasis. *Biochimica et Biophysica Acta, Molecular Cell Research*, 1864(9), 1459–1468. <https://doi.org/10.1016/j.bbamcr.2017.04.001>
- Barros, L. F. (2013). Metabolic signaling by lactate in the brain. *Trends in Neurosciences*, 36(7), 396–404. <https://doi.org/10.1016/j.tins.2013.04.002>
- Barros, L. F., & Deitmer, J. W. (2010). Glucose and lactate supply to the synapse. *Brain Research Reviews*, 63(1–2), 149–159. <https://doi.org/10.1016/j.brainresrev.2009.10.002>
- Bélanger, M., Allaman, I., & Magistretti, P. J. (2011). Brain energy metabolism: Focus on astrocyte-neuron metabolic cooperation. *Cell Metabolism*, 14(6), 724–738. <https://doi.org/10.1016/j.cmet.2011.08.016>
- Benador, I. Y., Veliova, M., Liesa, M., & Shirihai, O. S. (2019). Mitochondria bound to lipid droplets: Where mitochondrial dynamics regulate lipid storage and utilization. *Cell Metabolism*, 29(4), 827–835. <https://doi.org/10.1016/j.cmet.2019.02.011>
- Bennett, M. R., Farnell, L., & Gibson, W. G. (2005). A quantitative model of purinergic junctional transmission of calcium waves in astrocyte

- networks. *Biophysical Journal*, 89(4), 2235–2250. <https://doi.org/10.1529/biophysj.105.062968>
- Blanchette-Mackie, E. J., & Scow, R. O. (1983). Movement of lipolytic products to mitochondria in brown adipose tissue of young rats: An electron microscope study. *Journal of Lipid Research*, 24(3), 229–244.
- Brasaemle, D. L., & Wolins, N. E. (2012). Packaging of fat: An evolving model of lipid droplet assembly and expansion. *The Journal of Biological Chemistry*, 287(4), 2273–2279. <https://doi.org/10.1074/jbc.R111.309088>
- Brown, A. M., & Ransom, B. R. (2007). Astrocyte glycogen and brain energy metabolism. *Glia*, 55(12), 1263–1271. <https://doi.org/10.1002/glia.20557>
- Bruce, K. D., Zsombok, A., & Eckel, R. H. (2017). Lipid processing in the brain: A key regulator of systemic metabolism. *Frontiers in Endocrinology*, 8, 60. <https://doi.org/10.3389/fendo.2017.00060>
- Cabodevilla, A. G., Sánchez-Caballero, L., Nintou, E., Boiadjieva, V. G., Picatoste, F., Gubern, A., & Claro, E. (2013). Cell survival during complete nutrient deprivation depends on lipid droplet-fueled β -oxidation of fatty acids. *The Journal of Biological Chemistry*, 288(39), 27777–27788. <https://doi.org/10.1074/jbc.M113.466656>
- Chaves, V. E., Frasson, D., & Kawashita, N. H. (2011). Several agents and pathways regulate lipolysis in adipocytes. *Biochimie*, 93(10), 1631–1640. <https://doi.org/10.1016/j.biochi.2011.05.018>
- Chaves-Filho, A. B., Pinto, I. F. D., Dantas, L. S., Xavier, A. M., Inague, A., Faria, R. L., ... Miyamoto, S. (2019). Alterations in lipid metabolism of spinal cord linked to amyotrophic lateral sclerosis. *Scientific Reports*, 9(1), 11642. <https://doi.org/10.1038/s41598-019-48059-7>
- Cole, N. B., Murphy, D. D., Grider, T., Rueter, S., Brasaemle, D., & Nussbaum, R. L. (2002). Lipid droplet binding and oligomerization properties of the Parkinson's disease protein alpha-synuclein. *The Journal of Biological Chemistry*, 277(8), 6344–6352. <https://doi.org/10.1074/jbc.M108414200>
- de Castro Abrantes, H., Briquet, M., Schmuziger, C., Restivo, L., Puyal, J., Rosenberg, N., ... Chatton, J. Y. (2019). The lactate receptor HCAR1 modulates neuronal network activity through the activation of G. *The Journal of Neuroscience*, 39(23), 4422–4433. <https://doi.org/10.1523/JNEUROSCI.2092-18.2019>
- Derk, J., Bermudez Hernandez, K., Rodriguez, M., He, M., Koh, H., Abedini, A., ... Schmidt, A. M. (2018). Diaphanous 1 (DIAPH1) is highly expressed in the aged human medial temporal cortex and Upregulated in myeloid cells during Alzheimer's disease. *Journal of Alzheimer's Disease*, 64(3), 995–1007. <https://doi.org/10.3233/JAD-180088>
- Dienel, G. A. (2012). Brain lactate metabolism: The discoveries and the controversies. *Journal of Cerebral Blood Flow and Metabolism*, 32(7), 1107–1138. <https://doi.org/10.1038/jcbfm.2011.175>
- Dienel, G. A. (2019a). Brain glucose metabolism: Integration of energetics with function. *Physiological Reviews*, 99(1), 949–1045. <https://doi.org/10.1152/physrev.00062.2017>
- Dienel, G. A. (2019b). Does shuttling of glycogen-derived lactate from astrocytes to neurons take place during neurotransmission and memory consolidation? *Journal of Neuroscience Research*, 97(8), 863–882. <https://doi.org/10.1002/jnr.24387>
- Dienel, G. A., & Cruz, N. F. (2016). Aerobic glycolysis during brain activation: Adrenergic regulation and influence of norepinephrine on astrocytic metabolism. *Journal of Neurochemistry*, 138(1), 14–52. <https://doi.org/10.1111/jnc.13630>
- DiNuzzo, M., Mangia, S., Maraviglia, B., & Giove, F. (2010). Glycogenolysis in astrocytes supports blood-borne glucose channeling not glycogen-derived lactate shuttling to neurons: Evidence from mathematical modeling. *Journal of Cerebral Blood Flow and Metabolism*, 30(12), 1895–1904. <https://doi.org/10.1038/jcbfm.2010.151>
- Dinuzzo, M., Mangia, S., Maraviglia, B., & Giove, F. (2012). The role of astrocytic glycogen in supporting the energetics of neuronal activity. *Neurochemical Research*, 37(11), 2432–2438. <https://doi.org/10.1007/s11064-012-0802-5>
- Dong, J. H., Chen, X., Cui, M., Yu, X., Pang, Q., & Sun, J. P. (2012). beta2-adrenergic receptor and astrocyte glucose metabolism. *Journal of Molecular Neuroscience*, 48(2), 456–463. <https://doi.org/10.1007/s12031-012-9742-4>
- Duncan, R. E., Ahmadian, M., Jaworski, K., Sarkadi-Nagy, E., & Sul, H. S. (2007). Regulation of lipolysis in adipocytes. *Annual Review of Nutrition*, 27, 79–101. <https://doi.org/10.1146/annurev.nutr.27.061406.093734>
- Etschmaier, K., Becker, T., Eichmann, T. O., Schweinzer, C., Scholler, M., Tam-Amersdorfer, C., ... Panzenboeck, U. (2011). Adipose triglyceride lipase affects triacylglycerol metabolism at brain barriers. *Journal of Neurochemistry*, 119(5), 1016–1028. <https://doi.org/10.1111/j.1471-4159.2011.07498.x>
- Falchi, A. M., Sogos, V., Saba, F., Piras, M., Congiu, T., & Piludu, M. (2013). Astrocytes shed large membrane vesicles that contain mitochondria, lipid droplets and ATP. *Histochemistry and Cell Biology*, 139(2), 221–231. <https://doi.org/10.1007/s00418-012-1045-x>
- Falkowska, A., Gutowska, I., Goschorska, M., Nowacki, P., Chlubek, D., & Baranowska-Bosiacka, I. (2015). Energy metabolism of the brain, including the cooperation between astrocytes and neurons, especially in the context of glycogen metabolism. *International Journal of Molecular Sciences*, 16(11), 25959–25981. <https://doi.org/10.3390/ijms161125939>
- Farmer, B. C., Klumper, J., & Johnson, L. A. (2019). Apolipoprotein E4 alters astrocyte fatty acid metabolism and lipid droplet formation. *Cell*, 8(2), 182. <https://doi.org/10.3390/cells8020182>
- Fowler, P. C., Garcia-Pardo, M. E., Simpson, J. C., & O'Sullivan, N. C. (2019). Neurodegeneration: The central role for ER contacts in neuronal function and axonopathy, lessons from hereditary spastic paraplegias and related diseases. *Frontiers in Neuroscience*, 13, 1051. <https://doi.org/10.3389/fnins.2019.01051>
- Freyre, C. A. C., Rauher, P. C., Ejsing, C. S., & Klemm, R. W. (2019). MIGA2 links mitochondria, the ER, and lipid droplets and promotes De novo Lipogenesis in adipocytes. *Molecular Cell*, 76(5), 811–825.e814. <https://doi.org/10.1016/j.molcel.2019.09.011>
- Furuta, E., Pai, S. K., Zhan, R., Bandyopadhyay, S., Watabe, M., Mo, Y. Y., ... Watabe, K. (2008). Fatty acid synthase gene is up-regulated by hypoxia via activation of Akt and sterol regulatory element binding protein-1. *Cancer Research*, 68(4), 1003–1011. <https://doi.org/10.1158/0008-5472.can-07-2489>
- Gao, Q., & Goodman, J. M. (2015). The lipid droplet—a well-connected organelle. *Frontiers in Cell and Development Biology*, 3, 49. <https://doi.org/10.3389/fcell.2015.00049>
- Gómez-Ramos, P., & Asunción Morán, M. (2007). Ultrastructural localization of intraneuronal Abeta-peptide in Alzheimer disease brains. *Journal of Alzheimer's Disease*, 11(1), 53–59. <https://doi.org/10.3233/jad-2007-11109>
- Grajchen, E., Hendriks, J. J. A., & Bogie, J. F. J. (2018). The physiology of foamy phagocytes in multiple sclerosis. *Acta Neuropathologica Communications*, 6(1), 124–124. <https://doi.org/10.1186/s40478-018-0628-8>
- Guo, M., Ma, X., Feng, Y., Han, S., Dong, Q., Cui, M., & Zhao, Y. (2019). In chronic hypoxia, glucose availability and hypoxic severity dictate the balance between HIF-1 and HIF-2 in astrocytes. *The FASEB Journal*, 33(10), 11123–11136. <https://doi.org/10.1096/fj.201900402RR>
- Guo, X., Namekata, K., Kimura, A., Harada, C., & Harada, T. (2017). ASK1 in neurodegeneration. *Advances in Biological Regulation*, 66, 63–71. <https://doi.org/10.1016/j.jbior.2017.08.003>
- Guzmán, M., & Blázquez, C. (2001). Is there an astrocyte-neuron ketone body shuttle? *Trends in Endocrinology and Metabolism*, 12(4), 169–173. [https://doi.org/10.1016/s1043-2760\(00\)00370-2](https://doi.org/10.1016/s1043-2760(00)00370-2)
- Guzmán, M., & Blázquez, C. (2004). Ketone body synthesis in the brain: Possible neuroprotective effects. *Prostaglandins, Leukotrienes, and Essential Fatty Acids*, 70(3), 287–292. <https://doi.org/10.1016/j.plefa.2003.05.001>



- Hamilton, L. K., Dufresne, M., Joppé, S. E., Petryszyn, S., Aumont, A., Calon, F., ... Fernandes, K. J. (2015). Aberrant lipid metabolism in the forebrain niche suppresses adult neural stem cell proliferation in an animal model of Alzheimer's disease. *Cell Stem Cell*, 17(4), 397–411. <https://doi.org/10.1016/j.stem.2015.08.001>
- Henne, W. M., Reese, M. L., & Goodman, J. M. (2018). The assembly of lipid droplets and their roles in challenged cells. *The EMBO Journal*, 37(12), e9894. <https://doi.org/10.15252/embj.201898947>
- Herms, A., Bosch, M., Reddy, B. J., Schieber, N. L., Fajardo, A., Ruperez, C., ... Pol, A. (2015). AMPK activation promotes lipid droplet dispersion on deetyrosinated microtubules to increase mitochondrial fatty acid oxidation. *Nature Communications*, 6, 7176. <https://doi.org/10.1038/ncomms8176>
- Hertz, L., Chen, Y., Gibbs, M. E., Zang, P., & Peng, L. (2004). Astrocytic adrenoceptors: A major drug target in neurological and psychiatric disorders? *Current Drug Targets. CNS and Neurological Disorders*, 3(3), 239–267.
- Horvat, A., Zorec, R., & Vardjan, N. (2016). Adrenergic stimulation of single rat astrocytes results in distinct temporal changes in intracellular Ca²⁺ and cAMP-dependent PKA responses. *Cell Calcium*, 59(4), 156–163. <https://doi.org/10.1016/j.ceca.2016.01.002>
- Huang, Y., Ainsley, J. A., Reijmers, L. G., & Jackson, F. R. (2013). Translational profiling of clock cells reveals circadianly synchronized protein synthesis. *PLoS Biology*, 11(11), e1001703. <https://doi.org/10.1371/journal.pbio.1001703>
- Ioannou, M. S., Jackson, J., Sheu, S. H., Chang, C. L., Weigel, A. V., Liu, H., ... Liu, Z. (2019). Neuron-astrocyte metabolic coupling protects against activity-induced fatty acid toxicity. *Cell*, 177(6), 1522–1535. <https://doi.org/10.1016/j.cell.2019.04.001>
- Islam, A., Kagawa, Y., Miyazaki, H., Shil, S. K., Umaru, B. A., Yasumoto, Y., ... Owada, Y. (2019). FABP7 protects astrocytes against ROS toxicity via lipid droplet formation. *Molecular Neurobiology*, 56, 5763–5779. <https://doi.org/10.1007/s12035-019-1489-2>
- Kamermans, A., Rijnsburger, M., Chakraborty, A., van der Pol, S., de Vries, H. E., & van Horsen, J. (2019). Reduced Angiopoietin-like 4 expression in multiple sclerosis lesions facilitates lipid uptake by phagocytes via modulation of lipoprotein-lipase activity. *Frontiers in Immunology*, 10, 950–950. <https://doi.org/10.3389/fimmu.2019.00950>
- Kawabori, M., & Yenari, M. A. (2015). Inflammatory responses in brain ischemia. *Current Medicinal Chemistry*, 22(10), 1258–1277.
- Kilwein, M. D., & Welte, M. A. (2019). Lipid droplet motility and organelle contacts. *Contact (Thousand Oaks)*, 2, 251525641989568. <https://doi.org/10.1177/2515256419895688>
- Kis, V., Barti, B., Lippai, M., & Sass, M. (2015). Specialized cortex glial cells accumulate lipid droplets in *Drosophila melanogaster*. *PLoS One*, 10, e0131250. <https://doi.org/10.1371/journal.pone.0131250>
- Kreft, M., Bak, L. K., Waagepetersen, H. S., & Schousboe, A. (2012). Aspects of astrocyte energy metabolism, amino acid neurotransmitter homeostasis and metabolic compartmentation. *ASN Neuro*, 4(3), AN20120007. <https://doi.org/10.1042/AN20120007>
- Kreft, M., Milisav, I., Potokar, M., & Zorec, R. (2004). Automated high through-put colocalization analysis of multichannel confocal images. *Computer Methods and Programs in Biomedicine*, 74(1), 63–67. [https://doi.org/10.1016/s0169-2607\(03\)00071-3](https://doi.org/10.1016/s0169-2607(03)00071-3)
- Krishnan, J., Suter, M., Windak, R., Krebs, T., Felley, A., Montessuit, C., ... Krek, W. (2009). Activation of a HIF1 α -PPAR γ axis underlies the integration of glycolytic and lipid anabolic pathways in pathologic cardiac hypertrophy. *Cell Metabolism*, 9(6), 512–524. <https://doi.org/10.1016/j.cmet.2009.05.005>
- Laurenti, G., Benedetti, E., D'Angelo, B., Cristiano, L., Cinque, B., Raysi, S., ... Cimini, A. (2011). Hypoxia induces peroxisome proliferator-activated receptor alpha (PPAR α) and lipid metabolism peroxisomal enzymes in human glioblastoma cells. *Journal of Cellular Biochemistry*, 112(12), 3891–3901. <https://doi.org/10.1002/jcb.23323>
- Lauritzen, K. H., Morland, C., Puchades, M., Holm-Hansen, S., Hagelin, E. M., Lauritzen, F., ... Bergersen, L. H. (2014). Lactate receptor sites link neurotransmission, neurovascular coupling, and brain energy metabolism. *Cerebral Cortex*, 24(10), 2784–2795. <https://doi.org/10.1093/cercor/bht136>
- Liu, C., Wu, J., Zhu, J., Kuei, C., Yu, J., Shelton, J., ... Lovenberg, T. W. (2009). Lactate inhibits lipolysis in fat cells through activation of an orphan G-protein-coupled receptor, GPR81. *The Journal of Biological Chemistry*, 284(5), 2811–2822. <https://doi.org/10.1074/jbc.M806409200>
- Liu, K., & Czaja, M. J. (2013). Regulation of lipid stores and metabolism by lipophagy. *Cell Death and Differentiation*, 20(1), 3–11. <https://doi.org/10.1038/cdd.2012.63>
- Liu, L., MacKenzie, K. R., Putluri, N., Maletić-Savatić, M., & Bellen, H. J. (2017). The glia-neuron lactate shuttle and elevated ROS promote lipid synthesis in neurons and lipid droplet accumulation in glia via APOE/D. *Cell Metabolism*, 26(5), 719–737. <https://doi.org/10.1016/j.cmet.2017.08.024>
- Liu, L., Zhang, K., Sandoval, H., Yamamoto, S., Jaiswal, M., Sanz, E., ... Bellen, H. J. (2015). Glial lipid droplets and ROS induced by mitochondrial defects promote neurodegeneration. *Cell*, 160(1–2), 177–190. <https://doi.org/10.1016/j.cell.2014.12.019>
- Magistretti, P. J., & Allaman, I. (2018). Lactate in the brain: From metabolic end-product to signalling molecule. *Nature Reviews. Neuroscience*, 19(4), 235–249. <https://doi.org/10.1038/nrn.2018.19>
- Marschallinger, J., Iram, T., Zardeneta, M., Lee, S. E., Lehallier, B., Haney, M. S., ... Wyss-Coray, T. (2020). Lipid-droplet-accumulating microglia represent a dysfunctional and proinflammatory state in the aging brain. *Nature Neuroscience*, 23, 194–208. <https://doi.org/10.1038/s41593-019-0566-1>
- Morales, P. E., Bucarey, J. L., & Espinosa, A. (2017). Muscle lipid metabolism: Role of lipid droplets and Perilipins. *Journal Diabetes Research*, 2017, 1789395. <https://doi.org/10.1155/2017/1789395>
- Morland, C., Lauritzen, K. H., Puchades, M., Holm-Hansen, S., Andersson, K., Gjedde, A., ... Bergersen, L. H. (2015). The lactate receptor, G-protein-coupled receptor 81/hydroxycarboxylic acid receptor 1: Expression and action in brain. *Journal of Neuroscience Research*, 93(7), 1045–1055. <https://doi.org/10.1002/jnr.23593>
- Mosienko, V., Teschemacher, A. G., & Kasparov, S. (2015). Is L-lactate a novel signaling molecule in the brain? *Journal of Cerebral Blood Flow and Metabolism*, 35, 1069–1075. <https://doi.org/10.1038/jcbfm.2015.77>
- Nakajima, S., Gotoh, M., Fukasawa, K., Murakami-Murofushi, K., & Kunugi, H. (2019). Oleic acid is a potent inducer for lipid droplet accumulation through its esterification to glycerol by diacylglycerol acyltransferase in primary cortical astrocytes. *Brain Research*, 1725, 146484. <https://doi.org/10.1016/j.brainres.2019.146484>
- Nguyen, T. B., Louie, S. M., Daniele, J. R., Tran, Q., Dillin, A., Zoncu, R., ... Olzmann, J. A. (2017). DGAT1-dependent lipid droplet biogenesis protects mitochondrial function during starvation-induced autophagy. *Developmental Cell*, 42(1), 9–21. <https://doi.org/10.1016/j.devcel.2017.06.003>
- North, R. A., & Verkhatsky, A. (2006). Purinergic transmission in the central nervous system. *Pflügers Archiv*, 452(5), 479–485. <https://doi.org/10.1007/s00424-006-0060-y>
- Novikoff, A. B., Novikoff, P. M., Rosen, O. M., & Rubin, C. S. (1980). Organellar relationships in cultured 3T3-L1 preadipocytes. *The Journal of Cell Biology*, 87(1), 180–196. <https://doi.org/10.1083/jcb.87.1.180>
- O'Donnell, J., Zeppenfeld, D., McConnell, E., Pena, S., & Nedergaard, M. (2012). Norepinephrine: A neuromodulator that boosts the function of multiple cell types to optimize CNS performance. *Neurochemical*

- Research, 37(11), 2496–2512. <https://doi.org/10.1007/s11064-012-0818-x>
- Olzmann, J. A., & Carvalho, P. (2019). Dynamics and functions of lipid droplets. *Nature Reviews. Molecular Cell Biology*, 20(3), 137–155. <https://doi.org/10.1038/s41580-018-0085-z>
- Opstad, K. S., Bell, B. A., Griffiths, J. R., & Howe, F. A. (2008). An investigation of human brain tumour lipids by high-resolution magic angle spinning 1H MRS and histological analysis. *NMR in Biomedicine*, 21(7), 677–685. <https://doi.org/10.1002/nbm.1239>
- Ouimet, M., Franklin, V., Mak, E., Liao, X., Tabas, I., & Marcel, Y. L. (2011). Autophagy regulates cholesterol efflux from macrophage foam cells via lysosomal acid lipase. *Cell Metabolism*, 13(6), 655–667. <https://doi.org/10.1016/j.cmet.2011.03.023>
- Panov, A., Orynbayeva, Z., Vavilin, V., & Lyakhovich, V. (2014). Fatty acids in energy metabolism of the central nervous system. *BioMed Research International*, 2014, 472459–472422. <https://doi.org/10.1155/2014/472459>
- Papadopoulos, C., Orso, G., Mancuso, G., Herholz, M., Gumeni, S., Tadepalle, N., ... Rugarli, E. I. (2015). Spastin binds to lipid droplets and affects lipid metabolism. *PLoS Genetics*, 11(4), e1005149. <https://doi.org/10.1371/journal.pgen.1005149>
- Pardo, L., Valor, L. M., Eraso-Pichot, A., Barco, A., Golbano, A., Hardingham, G. E., ... Galea, E. (2017). CREB regulates distinct adaptive transcriptional programs in astrocytes and neurons. *Scientific Reports*, 7(1), 6390. <https://doi.org/10.1038/s41598-017-06231-x>
- Pellerin, L., & Magistretti, P. J. (1994). Glutamate uptake into astrocytes stimulates aerobic glycolysis: A mechanism coupling neuronal activity to glucose utilization. *Proceedings of the National Academy of Sciences of the United States of America*, 91(22), 10625–10629. <https://doi.org/10.1073/pnas.91.22.10625>
- Pennetta, G., & Welte, M. A. (2018). Emerging links between lipid droplets and motor neuron diseases. *Developmental Cell*, 45(4), 427–432. <https://doi.org/10.1016/j.devcel.2018.05.002>
- Petan, T. (2020). Lipid droplets in cancer. In *Reviews of Physiology, Biochemistry and Pharmacology*. Berlin, Heidelberg: Springer. https://doi.org/10.1007/112_2020_51
- Petan, T., Jarc, E., & Jusovic, M. (2018). Lipid droplets in cancer: Guardians of fat in a stressful world. *Molecules*, 23(8), 1941. <https://doi.org/10.3390/molecules23081941>
- Pol, A., Gross, S. P., & Parton, R. G. (2014). Review: Biogenesis of the multifunctional lipid droplet: Lipids, proteins, and sites. *The Journal of Cell Biology*, 204(5), 635–646. <https://doi.org/10.1083/jcb.201311051>
- Ponath, G., Ramanan, S., Mubarak, M., Housley, W., Lee, S., Sahinkaya, F. R., ... Pitt, D. (2017). Myelin phagocytosis by astrocytes after myelin damage promotes lesion pathology. *Brain: A Journal of Neurology*, 140(2), 399–413. <https://doi.org/10.1093/brain/aww298>
- Potokar, M., Kreft, M., Pangrsic, T., & Zorec, R. (2005). Vesicle mobility studied in cultured astrocytes. *Biochemical and Biophysical Research Communications*, 329(2), 678–683. <https://doi.org/10.1016/j.bbrc.2005.02.030>
- Potokar, M., Stenovec, M., Kreft, M., Gabrijel, M., & Zorec, R. (2011). Physiopathologic dynamics of vesicle traffic in astrocytes. *Histology and Histopathology*, 26(2), 277–284.
- Proia, P., Di Liegro, C. M., Schiera, G., Fricano, A., & Di Liegro, I. (2016). Lactate as a metabolite and a regulator in the central nervous system. *International Journal of Molecular Sciences*, 17(9), 1450. <https://doi.org/10.3390/ijms17091450>
- Pu, J., Ha, C. W., Zhang, S., Jung, J. P., Huh, W. K., & Liu, P. (2011). Interatomic study on interaction between lipid droplets and mitochondria. *Protein & Cell*, 2(6), 487–496. <https://doi.org/10.1007/s13238-011-1061-y>
- Quintero, M., Cabañas, M. E., & Arús, C. (2007). A possible cellular explanation for the NMR-visible mobile lipid (ML) changes in cultured C6 glioma cells with growth. *Biochimica et Biophysica Acta*, 1771(1), 31–44. <https://doi.org/10.1016/j.bbali.2006.10.003>
- Rambold, A. S., Cohen, S., & Lippincott-Schwartz, J. (2015). Fatty acid trafficking in starved cells: Regulation by lipid droplet lipolysis, autophagy, and mitochondrial fusion dynamics. *Developmental Cell*, 32(6), 678–692. <https://doi.org/10.1016/j.devcel.2015.01.029>
- Rémy, C., Foulhé, N., Barba, I., Sam-Lai, E., Lahrech, H., Cucurella, M. G., ... Arús, C. (1997). Evidence that mobile lipids detected in rat brain glioma by 1H nuclear magnetic resonance correspond to lipid droplets. *Cancer Research*, 57(3), 407–414.
- Renois, B., Malone, B., Falgairolle, M., Munasinghe, J., Stadler, J., Sibilla, C., ... Blackstone, C. (2016). Reep1 null mice reveal a converging role for hereditary spastic paraplegia proteins in lipid droplet regulation. *Human Molecular Genetics*, 25(23), 5111–5125. <https://doi.org/10.1093/hmg/ddw315>
- Robenek, H., Hofnagel, O., Buers, I., Robenek, M. J., Troyer, D., & Severs, N. J. (2006). Adipophilin-enriched domains in the ER membrane are sites of lipid droplet biogenesis. *Journal of Cell Science*, 119(Pt 20), 4215–4224. <https://doi.org/10.1242/jcs.03191>
- Sanchez-Abarca, L. I., Taberero, A., & Medina, J. M. (2001). Oligodendrocytes use lactate as a source of energy and as a precursor of lipids. *Glia*, 36(3), 321–329.
- Schindelin, J., Arganda-Carreras, I., Frise, E., Kaynig, V., Longair, M., Pietzsch, T., ... Cardona, A. (2012). Fiji: An open-source platform for biological-image analysis. *Nature Methods*, 9(7), 676–682. <https://doi.org/10.1038/nmeth.2019>
- Schonfeld, P., & Reiser, G. (2013). Why does brain metabolism not favor burning of fatty acids to provide energy? Reflections on disadvantages of the use of free fatty acids as fuel for brain. *Journal of Cerebral Blood Flow and Metabolism*, 33(10), 1493–1499. <https://doi.org/10.1038/jcbfm.2013.128>
- Schott, M. B., Rasineni, K., Weller, S. G., Schulze, R. J., Sletten, A. C., Casey, C. A., & McNiven, M. A. (2017). β -Adrenergic induction of lipolysis in hepatocytes is inhibited by ethanol exposure. *The Journal of Biological Chemistry*, 292(28), 11815–11828. <https://doi.org/10.1074/jbc.M117.777748>
- Schulz, J. G., Laranjeira, A., Van Huffel, L., Gärtner, A., Vilain, S., Bastianen, J., ... Dotti, C. G. (2015). Glial β -oxidation regulates drosophila energy metabolism. *Scientific Reports*, 5, 7805. <https://doi.org/10.1038/srep07805>
- Schwartz, J. P., & Wilson, D. J. (1992). Preparation and characterization of type 1 astrocytes cultured from adult rat cortex, cerebellum, and striatum. *Glia*, 5(1), 75–80. <https://doi.org/10.1002/glia.440050111>
- Sekiya, M., Hiraishi, A., Touyama, M., & Sakamoto, K. (2008). Oxidative stress induced lipid accumulation via SREBP1c activation in HepG2 cells. *Biochemical and Biophysical Research Communications*, 375(4), 602–607. <https://doi.org/10.1016/j.bbrc.2008.08.068>
- Shaw, C. S., Jones, D. A., & Wagenmakers, A. J. (2008). Network distribution of mitochondria and lipid droplets in human muscle fibres. *Histochemistry and Cell Biology*, 129(1), 65–72. <https://doi.org/10.1007/s00418-007-0349-8>
- Singh, P., Jorgačevski, J., Kreft, M., Grubišić, V., Stout, R. F., Potokar, M., ... Zorec, R. (2014). Single-vesicle architecture of synaptobrevin2 in astrocytes. *Nature Communications*, 5, 3780. <https://doi.org/10.1038/ncomms4780>
- Singh, R., Kaushik, S., Wang, Y., Xiang, Y., Novak, I., Komatsu, M., ... Czaja, M. J. (2009). Autophagy regulates lipid metabolism. *Nature*, 458(7242), 1131–1135. <https://doi.org/10.1038/nature07976>
- Sotelo-Hitschfeld, T., Niemeyer, M. I., Mächler, P., Ruminot, I., Lerchundi, R., Wyss, M. T., ... Barros, L. F. (2015). Channel-mediated lactate release by K^+ -stimulated astrocytes. *Journal of Neuroscience*, 35(10), 4168–4178. <https://doi.org/10.1523/JNEUROSCI.5036-14.2015>
- Sun, J., Ye, X., Xie, M., & Ye, J. (2016). Induction of triglyceride accumulation and mitochondrial maintenance in muscle cells by lactate. *Scientific Reports*, 6, 33732. <https://doi.org/10.1038/srep33732>
- Tang, F., Lane, S., Korsak, A., Paton, J. F., Gourine, A. V., Kasparov, S., & Teschemacher, A. G. (2014). Lactate-mediated glia-neuronal signalling



- in the mammalian brain. *Nature Communications*, 5, 3284. <https://doi.org/10.1038/ncomms4284>
- Thiam, A. R., Farese, R. V., & Walther, T. C. (2013). The biophysics and cell biology of lipid droplets. *Nature Reviews. Molecular Cell Biology*, 14(12), 775–786. <https://doi.org/10.1038/nrm3699>
- Toprak, U., Hegedus, D., Doğan, C., & Güney, G. (2020). A journey into the world of insect lipid metabolism. *Archives of Insect Biochemistry and Physiology*, 104(2), e21682. <https://doi.org/10.1002/arch.21682>
- Tracey, T. J., Steyn, F. J., Wolvetang, E. J., & Ngo, S. T. (2018). Neuronal lipid metabolism: Multiple pathways driving functional outcomes in health and disease. *Frontiers in Molecular Neuroscience*, 11, 10–10. <https://doi.org/10.3389/fnmol.2018.00010>
- Tsacopoulos, M., & Magistretti, P. (1996). Metabolic coupling between glia and neurons. *The Journal of Neuroscience*, 16(3), 877–885. <https://doi.org/10.1523/jneurosci.16-03-00877.1996>
- Vardjan, N., Chowdhury, H. H., Horvat, A., Velebit, J., Malnar, M., Muhić, M., ... Zorec, R. (2018). Enhancement of Astroglial aerobic glycolysis by extracellular lactate-mediated increase in cAMP. *Frontiers in Molecular Neuroscience*, 11, 148. <https://doi.org/10.3389/fnmol.2018.00148>
- Velebit, J., Horvat, A., Smolič, T., Prpar Mihevc, S., Rogelj, B., Zorec, R., & Vardjan, N. (2020). Astrocytes with TDP-43 inclusions exhibit reduced noradrenergic cAMP and Ca²⁺ signaling and dysregulated cell metabolism. *Scientific Reports*, 10(1), 6003. <https://doi.org/10.1038/s41598-020-62864-5>
- Verkhratsky, A., & Nedergaard, M. (2018). Physiology of Astroglia. *Physiological Reviews*, 98(1), 239–389. <https://doi.org/10.1152/physrev.00042.2016>
- Walther, T. C., & Farese, R. V. (2012). Lipid droplets and cellular lipid metabolism. *Annual Review of Biochemistry*, 81, 687–714. <https://doi.org/10.1146/annurev-biochem-061009-102430>
- Welte, M. A. (2009). Fat on the move: Intracellular motion of lipid droplets. *Biochemical Society Transactions*, 37(Pt 5), 991–996. <https://doi.org/10.1042/BST0370991>
- Xiong, W. C., Okano, H., Patel, N. H., Blendy, J. A., & Montell, C. (1994). Repo encodes a glial-specific homeo domain protein required in the drosophila nervous system. *Genes & Development*, 8(8), 981–994. <https://doi.org/10.1101/gad.8.8.981>
- Zechner, R., Madeo, F., & Kratky, D. (2017). Cytosolic lipolysis and lipophagy: Two sides of the same coin. *Nature Reviews. Molecular Cell Biology*, 18(11), 671–684. <https://doi.org/10.1038/nrm.2017.76>
- Zoula, S., Rijken, P. F., Peters, J. P., Farion, R., Van der Sanden, B. P., Van der Kogel, A. J., ... Remy, C. (2003). Pimonidazole binding in C6 rat brain glioma: Relation with lipid droplet detection. *British Journal of Cancer*, 88(9), 1439–1444. <https://doi.org/10.1038/sj.bjc.6600837>

SUPPORTING INFORMATION

Additional supporting information may be found online in the Supporting Information section at the end of this article.

How to cite this article: Smolič T, Tavčar P, Horvat A, et al. Astrocytes in stress accumulate lipid droplets. *Glia*. 2021;69:1540–1562. <https://doi.org/10.1002/glia.23978>